ELSEVIER

Journal of Experimental Marine Biology and Ecology, 239 (1999) 85–124

JOURNAL OF EXPERIMENTAL MARINE BIOLOGY AND ECOLOGY

Detailing agents of physical disturbance: wave-induced velocities and accelerations on a rocky shore

Brian Gaylord*

Hopkins Marine Station of Stanford University, Pacific Grove, CA 93950, USA

Received 9 April 1998; received in revised form 11 February 1999; accepted 23 February 1999

Abstract

Water motion produced by breaking waves plays a defining role in structuring intertidal communities. However, despite the clear ecological importance of wave action, fine-scale details of the flows generated by breaking waves on rocky shores have not been well-described. This lack of information has hindered the efficacy of mechanistic studies aimed at exploring quantitatively the processes leading to wave-induced damage or mortality of organisms in littoral habitats. In response to these limitations, high-frequency field measurements of intertidal water velocities and accelerations were conducted simultaneously with recordings of inshore wave height at four representative sites in the mid-intertidal zone of a rocky shore. Maximum velocities and accelerations recorded under waves of measured height are presented and placed in the context of simple wave theories. Rates of occurrence of simultaneous velocities and accelerations are computed as a function of wave height, providing a means of linking instantaneous values of drag and lift to concurrent hydrodynamic accelerational forces. These data together provide an improved, high-resolution picture of the nature of flows typical of littoral environments and their relationship to wave height, and as such serve to reemphasize both the severity as well as the stochastic nature of the fluid motions that characterize wave-swept coasts.

Keywords: Acceleration; Drag; Exposure; Hydrodynamic forces; Velocity; Wave action; Wave height

1. Introduction

The intensity of wave action is one of the primary controlling agents determining the

*Present address: Dept. of Ecology, Evolution, and Marine Biology, University of California, Santa Barbara, CA 93106, USA. Tel.: +1-805-893-7397; fax: +1-893-3777.
E-mail address: gaylord@lifesci.ucsb.edu (B. Gaylord)

0022-0981/99/$ – see front matter
PII: S0022-0981(99)00031-3

structure of communities on many marine shores (Dayton, 1971, 1975; Levin and Paine, 1974, 1975; Menge, 1976, 1978; Lubchenco and Menge, 1978; Paine and Levin, 1981; Sousa, 1984, 1985; Menge and Farrell, 1989). In intertidal regions, species assemblages and the rates of turnover of both plants and animals may be influenced as much by the level of wave exposure typical of a site as by biological factors such as predation or competition (Lewis, 1964, 1968; Paine, 1979; Paine and Levin, 1981; McQuaid and Branch, 1985; Ricketts et al., 1985). Alternatively, wave action may interact critically with biological features to affect the persistence of organisms; for example by limiting the activity or distribution of important grazers and predators (Lubchenco and Menge, 1978; Menge, 1978; Underwood and Jernakoff, 1984), or by opening up new patches of substratum for colonization in an otherwise space-limited arena (Dayton, 1971; Paine and Levin, 1981; Sousa, 1984, 1985). However, despite the acknowledged importance of wave-induced water motion, the nature of the flows occurring in the surf zone of rocky shores (where productivity and species diversity are often highest (Connell, 1978; Leigh et al., 1987)) remains largely unquantified. Although information regarding nearshore wave dynamics exists for smooth, gently-sloping planar beaches (e.g., Thornton and Guza, 1982, 1983), the irregular topography and steep slopes of rocky shores produce exceptionally complicated flows that have as yet proven difficult to describe. Indeed, the complex variability in substrate contours on rocky coasts suggests that theoretical or analytical approaches for defining the fine-scale flows in these regions may be impossible. Empirical and statistical methods may therefore provide the only reasonable alternative.

Previous experimental attempts to quantify flow in intertidal habitats have focused on four basic methods: large scale predictions based on fetch parameters, time-integrated measures that yield estimates of overall water motion but reveal little about flow magnitude, the use of maximum force recording spring scales that provide information about peak flow rates during particular time intervals, and time series recordings that describe finer-scale temporal details of fluid motion. Fetch-related exposure indices rely on observed correlations between wind speed and the maximum distance wind can blow unimpeded across a stretch of open ocean (the fetch) to predict the size of the waves that can be produced (Thomas, 1986; Hummon, 1989; Brodersen, 1995). While exposure indices using fetch information are simple to compute and require no field manipulations, the resulting estimates are crude and provide limited spatial and temporal resolution (i.e., exposure levels averaged over kilometers and months). Alternatively, other researchers have placed in the field substances such as plaster of Paris that dissolve at rates that depend on the net flux of water past them (Muus, 1968; Doty, 1971). These dissolution techniques have proven useful for studies involving questions of mass/heat transfer or nutrient/particle delivery to and from organisms (Gerard, 1982; Koehl and Alberte, 1988), but provide little data regarding instantaneous flow magnitudes or imposed hydrodynamic forces. More effective for addressing issues of wave dislodgement are maximum force recording spring scales, which have been used with some success to estimate the peak velocities that occur in rocky intertidal regions (Jones and Demetropoulos, 1968; Bell and Denny, 1994). These devices are easily constructed, inexpensive, and therefore show considerable potential for wide-spread deployment and replicate categorization of a broad array of topographies. Unfortunately they are difficult

to calibrate in flows like those found intertidally; thus questions remain regarding the possibility that inertial forces associated with the response of the devices to flow may corrupt the accuracy of the readings. Higher-frequency, continuous flow recordings in intertidal regions of rocky coasts (Koehl, 1977; Denny, 1985) have perhaps the greatest potential for improving our understanding of fluid-organism interactions, but such studies are logistically difficult and therefore rarely attempted.

All four of the above methods are useful and have been effectively employed to address a variety of issues in ecology (e.g., Gerard, 1982; Denny et al., 1985; McEachreon and Thomas, 1987; Koehl and Alberte, 1988; Blanchette, 1997). However, the first three methods provide but a single datum to describe hydrodynamic processes occurring over some considerable length of time, and thus are incapable of providing information regarding the rate at which hydrodynamic forces are imposed, the direction or duration of flow, or the relationship between the height of a given wave and the water motion it produces. Higher-frequency recordings are more effective in addressing such issues, but of the few such studies actually conducted, only those of Denny (1985) and Denny et al. (1985) possess sufficient temporal resolution to effectively characterize the rapid velocity fluctuations typical of intertidal regions. In addition and perhaps most importantly, no previous experimental work has attempted to define the multiple relationships among intertidal water velocity, acceleration, and inshore wave height on steep rocky shores. The lack of information concerning these relationships has greatly limited the development of mechanistic predictions regarding the consequences of wave action for intertidal plants and animals (Denny et al., 1985; Gaylord et al., 1994).

In view of this need for additional empirical data, high-frequency measurements were conducted of water velocities and accelerations under breaking waves on a rocky shore. Robust miniature drag sphere flow probes were used as a low-cost alternative to the velocity-measuring devices traditionally employed by nearshore oceanographers and fluid dynamicists (e.g., electromagnetic current meters, acoustic doppler flow meters, and hot-film anemometers), due to the high risk of equipment damage, and because of practical difficulties associated with each of these methods (e.g., poor spatial and/or temporal resolution, immersion spiking, attenuation from entrained air, and signal corruption from bubbles and fouling). Recordings of inshore wave height were also conducted simultaneously with the flow measurements, allowing for exploration of the relationships between local wave height, velocity, and acceleration. This empirical approach provides first-order physical data useful to ecologists in evaluating disturbance dynamics, without invoking the complexity of full-blown wave theories that depend on parameters that are often difficult to determine for rocky shores with irregular topography.

2. Theory

2.1. Ocean waves

Wind-generated sea waves propagate with little energy loss across the water's surface until they encounter land. In the limiting case where waves of a narrow band of

frequency and random phase interact (a situation often produced when waves arrive at a site from a region of ocean some distance away), their heights are distributed according to a Rayleigh probability density function (Longuet-Higgins, 1952):

$$p(H) = \frac{2H}{H_{\mathrm{rms}}^2} \exp\left[-\left(\frac{H}{H_{\mathrm{rms}}} \right)^2 \right], \tag{1}$$

where the wave height, H, is twice the amplitude of the waveform and H_{rms} is the root mean square wave height (Table 1). Long-period swell, which usually includes the largest waves that impinge on a shore, is commonly generated by storms blowing across large expanses of open ocean many kilometers distant; thus swell heights are usually well represented by the Rayleigh distribution. The shape of the Rayleigh distribution is presented in Fig. 1, showing the characteristic right hand (large-wave) tail and the relative position of the single specifying parameter, H_{rms}.

2.2. Surf-zone flows

When waves reach land, they steepen, increase in height, and subsequently break (see U.S. Army Corps of Engineers, 1984, or Denny, 1988 for details). This process may modify the incident wave height distribution and also affects strongly the nature of the

Table 1
Symbols

A	Area projected along the axis of flow, m^2
C	Wave speed, m/s
C_a	Added mass coefficient, nondimensional
C_d	Drag coefficient, nondimensional
d	Water depth, m
$(du/dt)_{\mathrm{max}}$	Maximum acceleration during a wave, m/s^2
D	Sphere diameter, m
F	Force, N
F_x	Shoreward-seaward force component, N
F_y	Alongshore force component, N
g	Acceleration due to gravity, 9.81 m/s^2
H	Wave height, m
H_s	Significant wave height, m
H_{rms}	Root mean square wave height, m
k	Roughness height, m
L	Wavelength, m
t	Time, s
u	Velocity, m/s
u_{max}	Maximum velocity in a wave, m/s
u_x	Shoreward-seaward velocity component, m/s
u_y	Alongshore velocity component, m/s
V	Volume, m^3
ρ	Fluid density, kg/m^3
τ	Wave period, s
Φ	Pressure, N/m^2

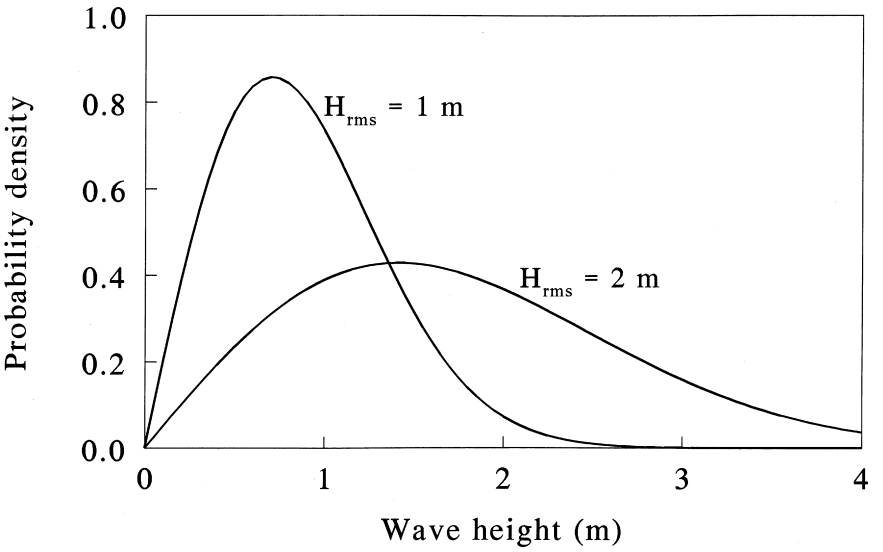

Fig. 1. Rayleigh probability density curve of wave height. H_{rms} completely defines the shape of the distribution. Example curves for two rms wave heights are shown.

water motion produced by the waves. While waves outside the breaker zone generate regular and predictable orbital flows, fluid trajectories under breaking waves become rapidly and energetically disorganized due to turbulent degeneration of the waveform. As breaking continues, waves typically evolve into steep-faced turbulent bores which propagate through the surf zone with speed, C, described by the first-order terms of solitary wave theory (Munk, 1949):

$$C \cong \sqrt{g(H + d)}, \tag{2}$$

where g is the acceleration due to gravity and d is water depth. The largest fluid velocities associated with bores occur near their crests, with magnitudes approaching C.

Unfortunately, Eq. 2 cannot be rigorously applied to waves in the shallowest regions of the surf zone or in the swash zone (the region on the shore above mean water level) because solitary wave theory is based on a series expansion which includes higher-order terms with depth in the denominator. This causes the untruncated form of Eq. 2 to deviate from physical reality as d goes to zero. A variety of alternative bore theories (most of which match Eq. 2 to first order (Boussinesq, 1872, cited in Komar, 1976; McCowan, 1891; Keller et al., 1960; Shen and Meyer, 1963)) have similar physically unreasonable limitations when applied to water of negligible depth. As a consequence, a consensus wave theory for use in exceptionally shallow water remains unavailable, and no analytical expressions have become standard for the swash.

Numerical and experimental approaches, however, provide data with which to develop approximate estimates for wave propagation speeds and bulk fluid velocities in exceptionally shallow water and in the swash zone. For example, Van Dorn (1976, 1978)

presents laboratory experiments that suggest breaking waves travel at rates of about $\sqrt{1.5gH}$ in shallow water, while lab and field experiments (LeMehaute et al., 1968; Van Dorn, 1978; Hedges and Kirkgoz, 1981) indicate that bulk water velocities (i.e., velocities associated with the overall motion of the bore rather than with eddies produced by breaking) near the substratum under breaking waves are typically about 0.4 times the wave speed. Hibberd and Peregrine (1979) develop a numerical model for a uniform bore running up a (potentially steep) beach face that predicts maximum velocities equal to twice the wave speed. Taken together, these data suggest that water velocities (u) near the seabed under breaking waves traveling through water where $H \gg d$ or through the swash may vary roughly as:

$$u \sim \sqrt{gH}, \tag{3}$$

which conveniently enough is what one would compute from Eq. 2 simply by setting d to zero (e.g., as in Denny, 1995). Note that although Eq. 3 may describe bulk water velocities associated with the passage of a bore itself, the chaotic localized flows produced by the action of wave breaking (which are superimposed on the waveform velocities) are too complex and variable to express analytically. Thus empirical and statistical methods must be employed to describe surf-zone velocities in any detail. There are no generally accepted theories for predicting fluid accelerations under breaking waves.

2.3. Hydrodynamic forces

Both water velocities and water accelerations have the potential to impose forces on organisms. Drag and lift are forces that result from the velocity of the water relative to a plant or animal, and have magnitudes that depend on the square of the relative velocity. Of these two velocity-dependent forces, drag acts along the axis of flow, and lift perpendicular to it. Each varies in proportion to a characteristic area of an organism. Vogel (1981) and Denny (1988) provide more complete discussions of these fluid forces and their biological importance.

A second category of fluid force results from water acceleration. This hydrodynamic accelerational force increases linearly with the magnitude of the relative water acceleration and varies in proportion to an organism's volume rather than its area. Denny et al. (1985) and Gaylord et al. (1994) discuss potential theoretical consequences of the difference in areal versus volumetric scaling between drag and the hydrodynamic accelerational force. They also note the need for an improved understanding of the relationship between water velocity and acceleration due to this capacity of both components of fluid motion to impose forces independently but simultaneously.

3. Materials and methods

3.1. Flow probes

Water motion in the surf zone was measured using four 2-axis, cantilever-style

drag-sphere flow probes (Fig. 2), similar in principle to that of Donelan and Motycka (1978). Their basic design was as follows. A 1.52 cm diameter, roughened spherical drag element was mounted on the tip of a vertically-oriented 2.4 mm diameter stainless steel rod, the base of which was rigidly fixed to a set of two orthogonal double-beam aluminum cantilevers. Horizontal forces applied to the drag sphere deflected the cantilevers and this deformation was sensed by semiconductor strain gauges (MicroGage 919) mounted on the beams. The gauges were configured as wheatstone bridges (Horowitz and Hill, 1989), providing voltage signals proportional to force. Due to the large gauge factor characteristic of semiconductor strain gauges (140), very stiff cantilevers could be used, allowing for a fast time response (the natural frequency of the probes in seawater was 450 Hz, determined by plucking a submerged probe's drag element and recording the voltage trace of its resulting damped, free vibration) without requiring excessive signal amplification. Each of the cantilevers responded to forces applied along one of two mutually perpendicular horizontal axes. The double beam structure of the cantilevers reduced cross-talk between these two axes to less than 1%. The entire device was waterproofed and enclosed in a protective housing. Shielded instrumentation cable supplied power and carried the signals from probe to computer.

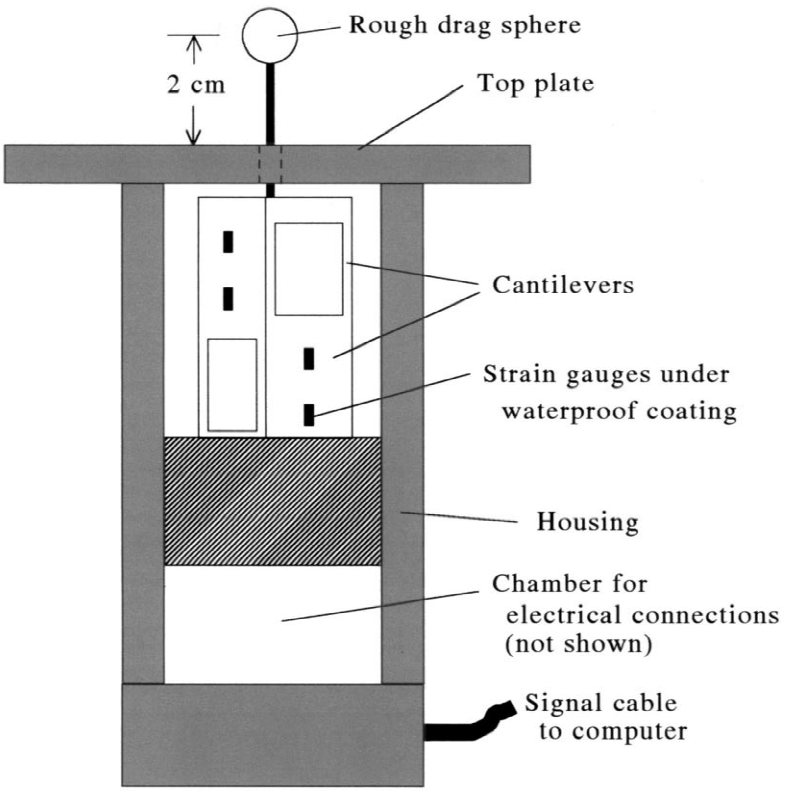

Fig. 2. Schematic of a drag sphere flow probe.

Calibration of the probes proceeded in three steps. First, the voltage signal versus force relationship for the probes was determined by positioning the probes horizontally, hanging weights from the center of their drag spheres, and regressing the resulting change in voltage against the applied force. This procedure was repeated for both axes of each probe. Voltage-force calibrations were completed with the probes at seawater temperature since semiconductor strain gauges are temperature sensitive (this effect was minimized by using matched sets of four gauges). Second, the link between force and velocity was defined by measuring the drag coefficient (C_d; see Flow record analysis, below) of the drag spheres under both steady and accelerating flow conditions. The two sets of apparatus used and associated analysis techniques are described in Denny and Gaylord (1996) (but note that the second right hand term in their Eqs. 7 and 8 was mistyped and be should be $C_a\rho Va$). The C_d of the drag spheres was 0.83 for both types of flow. As expected, due to the exceptional surface roughness (roughness ratio $k/D=1/15$, where k is the height of the roughness elements and D is the sphere diameter; see Schlichting, 1979) of the drag spheres, this value was substantially larger than the standard C_d of 0.5 typically given for smooth spheres in flows of low turbulence. The surface roughness also eliminated any evidence of the turbulent boundary layer transition and associated reduction in C_d that routinely occurs for smooth spheres in the vicinity of $\mathrm{Re}\sim10^5$ (Schlichting, 1979). Third, the overall velocity calibration was verified in the field against a Marsh–McBirney 511 electromagnetic (EM) current meter using a modification of the boat-tow device of Utter and Denny (1996). A representative example of this overall calibration is shown in Fig. 3. Note that the scatter of points from the drag sphere probe is not noise but rather reflects the probe's ability to respond to localized, rapid turbulent fluctuations which the time- and spatially-averaging EM current meter cannot resolve. If output from the drag sphere probe were low-pass filtered, the measured data points would fall almost exactly on the force curve predicted by the averaging EM flowmeter.

3.2. Field sites

The flow probes described above were placed at four different sites in the mid-intertidal zone along the shoreline of Hopkins Marine Station, Pacific Grove, California. Each of these sites is typical of many rocky intertidal locations, with complex topography characterized by non-uniform slope and variability in substrate elevation that occurs across multiple spatial scales. All sites are located near or within beds of the mussel, *Mytilus californianus*, and can be categorized as being moderately exposed (in the criteria of Ricketts et al., 1985).

Site 1 (Fig. 4a) is located just shoreward and above a low-intertidal tide pool that interrupts a mostly planar, sloping incline (ignoring centimeter-scale irregularities) that runs from subtidal depths to the high-intertidal zone. This incline forms a spur protruding between adjacent surge channels and faces directly toward the dominant direction of oncoming swell. It therefore experiences powerful plunging breakers during storms.

Site 2 (Fig. 4b) is located on the seaward edge of a rock bench, which drops sharply just offshore to form a submerged 5 m step. This step causes waves at this site to shoal

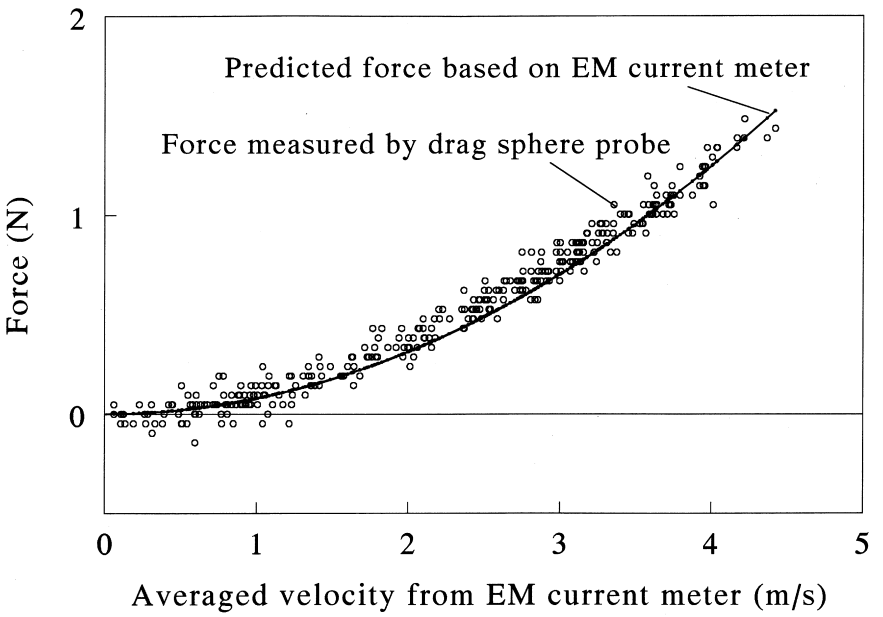

Fig. 3. Representative calibration curve for one axis of a drag sphere flow probe. Note that because this calibration was conducted in the field in complex flows, much of the scatter around the predicted curve is an expected consequence of the better spatial and temporal resolution of the flow probe relative to the coarser, temporally and spatially averaged estimates of the electromagnetic (EM) current meter.

rapidly and break almost immediately. Because this site sits directly at the point of breaking, it encounters large waves at their peak height. A second, smaller step shoreward and above the rock bench forces water to move parallel to the shore, with the result that this site often experiences strong alongshore flow late in a wave cycle. Also, during exceptionally high tides, surging waves may reflect off this upper step.

Site 3 (Fig. 4c) sits on a slight elevation above a broad, open region of horizontal substratum, 2.5 m in front of a 3 m high vertical face. The waves at this site are predominantly of the spilling type and break somewhat seaward of the probe, forming classical turbulent bores that subsequently run shoreward to interact with the sensors.

Site 4 (Fig. 4d) sits within a narrow seaward-directed channel that slopes downward almost uniformly from the high-intertidal zone to subtidal depths. The waves impinging on this site are similar to those impacting site 1.

3.3. Deployment and sampling

Field measurements of flow were completed as follows. Rigid concrete emplacements were built into the rock at each of the four sites described above. The emplacements were constructed such that the top plate of the probe housing could be bolted down flush with the surrounding rock, with the probe's drag sphere positioned 2 cm above the substratum. This placed the drag sphere above the substratum at an elevation similar to

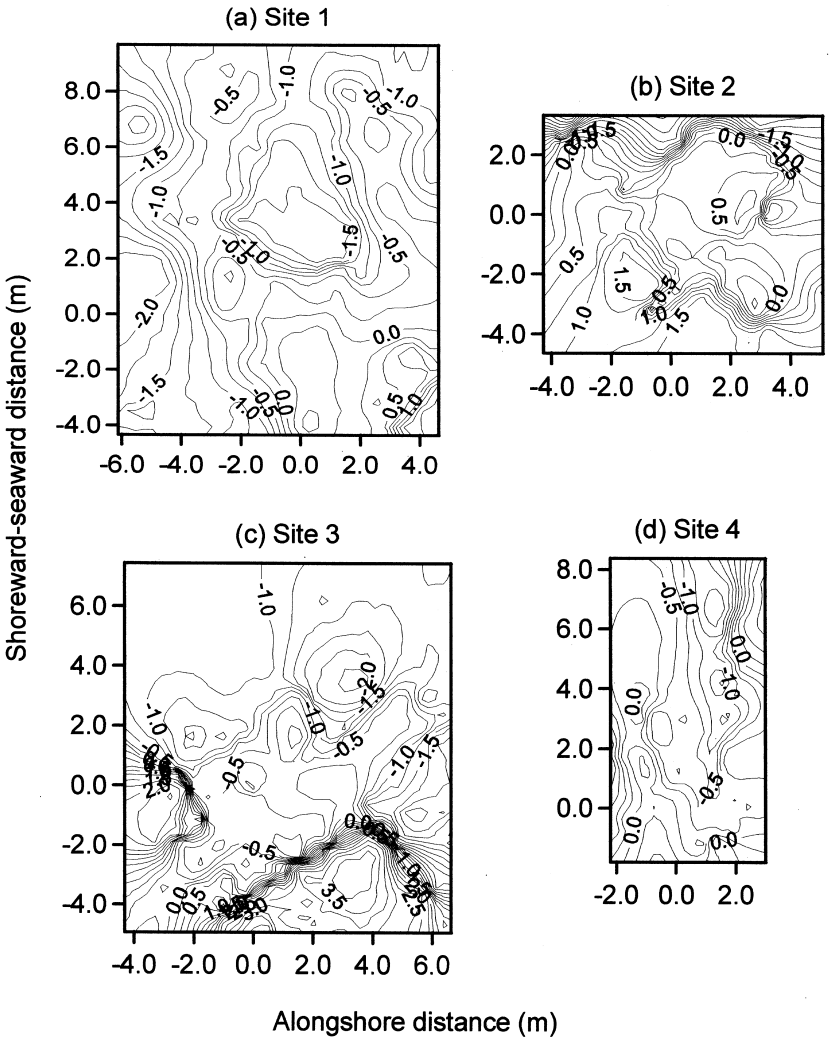

Fig. 4. Topography of the intertidal sites used for the flow recordings. At each site, the probe was positioned at (*x*, *y*, *z*) reference coordinates of (0,0,0). Seaward points toward the top of the page, and elevations (*z*) and horizontal distances are in meters. (a) Site 1. (b) Site 2. (c) Site 3. (d) Site 4.

the height of many intertidal seaweeds and invertebrates. One axis of the probe was oriented to sense shoreward-seaward water motion, while the other measured alongshore flow. The signal cable of the probe was run from the surf zone, where it was tied down to a series of eyebolts screwed into the rock, up away from the shore to the laboratory 100 m distant. In the laboratory, the signals were amplified, passed through an analog to digital converter, and recorded by computer.

The height of the waves passing over the probes was measured using a pressure transducer (Omega PX176) mounted in a waterproof housing. A secondary emplacement

was constructed at each field site to hold this transducer, located in all cases within 0.5 m of the flow probe at a given site. When deployed in one of these emplacements, the pressure transducer was held flush with the seabed and its signal cable was strung alongside that of the adjacent flow probe up through the surf zone to the laboratory for simultaneous recording. Because only a single pressure transducer was available, it was rotated among sites on different recording days.

A subtidal wave meter (Ocean Sensors OS100) located 50 m offshore in 12 m of water provided a record of sea surface elevation outside the surf zone during the same period sampled by the intertidal flow probes and pressure transducer. This allowed for a comparison of the unbroken wave height distribution to the inshore heights of broken waves. The records from this device, however, are incomplete; thus only some of the recording sessions include the 12 m depth data.

A concerted effort was made to deploy the instruments during extreme weather events when waves were large. Although many such events did not coincide with low tides, preventing access to (and measurements at) the intertidal field sites, the data collected do include recordings from among some of the more severe winter storms of 1995 and 1996. To gather flow information across a range of sea states, measurements were also completed during moderate and relatively calm conditions.

When making measurements, the analog signals from the flow probes and intertidal pressure transducer were sampled at 2000 Hz through multiple 20 s intervals. Each 20 s data stream was written to disk, and sampling of the subsequent 20 s interval was initiated immediately following. This process was continued until computer storage was exhausted, providing a near-continuous record of flow conditions spanning approximately 40 minutes. Due to the high volume of data sampled per time, typically only a single 40 minute session was recorded per tidal cycle. Recordings were made at high tide during 28 separate tidal cycles, encompassing a variety of high-tide amplitudes and sea states, on 21 different days during the period from January 1995 through August 1996. Of the 28 intertidal flow recording sessions, 11 were synchronized with 2048-point, 1 Hz recordings from the subtidal wave meter.

3.4. Flow record analysis

Following recording and storage, each 20 s intertidal flow interval was digitally low-pass filtered at 300 Hz to eliminate any high-frequency components of the raw signal that might have arisen from vibration of the probe at its natural frequency. Note that although no analog filters were used, inertial damping of the probe eliminates substantial signal energy at frequencies above approximately 750 Hz (verified in preliminary 5000 Hz power spectra), preventing high-frequency aliasing for the 2000 Hz sample rate used.

Once filtered, the shoreward-seaward and alongshore flow probe signals during each sample interval were converted to force, and the intertidal pressure measurements (filtered at 30 Hz) were converted to water depth using the relation:

$$d = \frac{\Phi}{\rho g} \tag{4}$$

where Φ is pressure. Measurements from the subtidal wave gauge were corrected for depth attenuation using standard spectral methods (Kinsman, 1965) to yield a description of the sea surface elevation through time. From this information, the 12 m depth rms wave height during the sampling period was calculated as (Longuet-Higgins, 1980; Thornton and Guza, 1982):

$$H_{\mathrm{rms}} = \sqrt{8\sigma^2} \tag{5}$$

where σ^2 is the variance of the sea surface elevation. This value was then divided by the shoaling coefficient (derived from linear wave theory, U.S. Army Corps of Engineers, 1984) for waves of the dominant period arriving during the 12 m deep subtidal measurements, providing a rough estimate of the deep-water H_{rms} value for the recording period. This correction was always less than 5%.

Because the flow probes and pressure transducer were situated in the mid-intertidal zone above mean water level (i.e., in the upper surf zone or lower swash zone depending on the tide), the probes were commonly emersed (i.e., exposed to air) during the backwash between waves. Therefore d in Eq. 4 equals the height of the waves passing over a probe. Emersion of the probes immediately prior to the arrival of a wave also meant that the probes encountered impact-type forces during the early stages of a wave cycle, in addition to the expected drag and hydrodynamic accelerational forces. Because impact forces are notoriously difficult to express as functions of the magnitude of impinging water velocities (Schmidt et al., 1992), no attempt was made to develop estimates of water velocity or acceleration from force measurements made during the first 0.5 s of the passing waves. The 0.5 s cutoff was chosen (based on observations that the majority of impact-type forces occurred during the first 0.05 s of wave arrival) as a conservative blanking window for eliminating potentially biased estimates from the flow records. Note, however, that although these wave impact segments were excluded from the compiled flow data, their omission in no way implies that the underlying impact-type forces themselves are biologically unimportant. Because a repeatable zero-force reading existed for nearly every wave (during emersion of the probe), the instants of wave arrival within each 20 s interval were easily detected visually, to the nearest 10 msec, from plots of force versus time. This visual method was reliable and avoided many of the complications associated with the use of standard zero-upcrossing methods (e.g., Thornton and Guza, 1983) that are often employed for continuously-submerged sensors.

Impact-type forces were not observed after the first 0.5 s of a wave; thus during the remaining portion of a wave cycle the instantaneous total horizontal force applied to a probe was assumed to arise from the sum of drag and hydrodynamic accelerational forces. That is:

$$F(t) = \frac{1}{2}\,\rho A\, C_d\, u|u| + (1 + C_a)\rho V \frac{\mathrm{d}u}{\mathrm{d}t}, \tag{6}$$

one form of the so-called ‘‘Morison equation’’ (Morison et al., 1950). The first term on the right hand side of Eq. 6 represents the hydrodynamic contribution of drag (Vogel, 1981), while the second term includes the summed contributions of virtual buoyancy (a force arising from the pressure gradient associated with an accelerating fluid; Batchelor,

1967), and the added mass force (imposed due to the temporal alteration of momentum occurring when a changing flow field is diverted around an object; Milne-Thomson, 1968). A is the frontal area of the drag sphere, C_d the empirically-measured drag coefficient (a velocity shape factor), C_a an accelerational shape factor termed the added mass coefficient, V the volume of the sphere, and t time. The absolute value sign is used to account for directionality of the flow. Due to the presence of the second term on the right hand side of Eq. 6, intertidal flow speeds cannot be simply calculated algebraically from the force measurements. Instead, a more complicated procedure must be used to extract from the force records simultaneous values of water velocity and water acceleration through time. The technique used to accomplish this is a variation of that developed by Denny et al. (1985). The total force of Eq. 6 is decomposed into shoreward-seaward and alongshore components, yielding:

$$F_x(t) = \frac{1}{2}\,\rho A\, C_d \sqrt{u_x^2 + u_y^2}\, u_x + (1 + C_a)\,\rho V \frac{\mathrm{d}u_x}{\mathrm{d}t}, \tag{7}$$

$$F_y(t) = \frac{1}{2}\,\rho A\, C_d \sqrt{u_x^2 + u_y^2}\, u_y + (1 + C_a)\,\rho V \frac{\mathrm{d}u_y}{\mathrm{d}t}, \tag{8}$$

where $F_x(t)$ and $F_y(t)$ are known quantities, each measured by one axis of a flow probe. These equations can be solved numerically for u_x, u_y, $\mathrm{d}u_x/\mathrm{d}t$, and $\mathrm{d}u_y/\mathrm{d}t$ through time, here via a 4th-order Runge–Kutta technique (Press et al., 1992). When applied to the field flow probe measurements, this procedure yields a description of the variation of both water velocity and water acceleration through time at the location of the probe (i.e., Eulerian time series), in both the seaward-shoreward and alongshore directions, with 1000 Hz temporal resolution.

3.5. Compilation of the data

The data from the 28 intertidal recording sessions were processed to address five issues:

3.5.1. Wave height distributions

Intertidal wave height distributions from each of the recording sessions were calculated and compared to theoretical Rayleigh distributions with the same rms wave height.

3.5.2. Water velocity versus inshore wave height

Waves from different recording sessions were placed in one of two crude classifications based on visual observations of their general manner of breaking, and the relationship between surf-zone velocity and inshore wave height was explored for both of these classifications at each of the four intertidal field sites. The first classification was composed of ''*newly breaking*'' waves (Fig. 5a). A wave of this sort had a crest that had become unstable and was beginning to plunge or spill down the face of the wave, but the resulting jet or roller had not yet affected the base of the wave when it impinged on the flow probe. In contrast, waves interacting with the flow probe for which the jet or roller

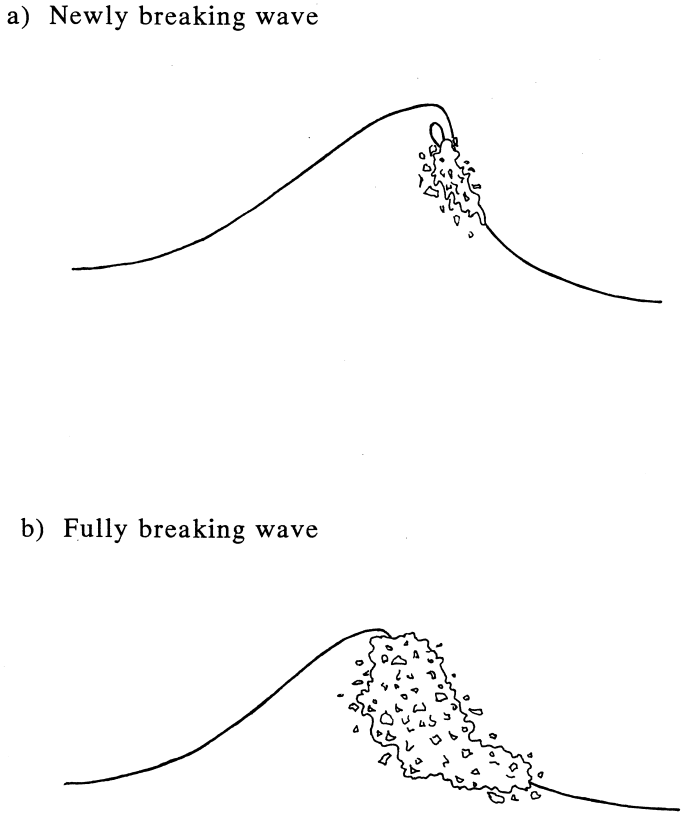

Fig. 5. Schematic of the two crude classes of breaking waves observed at the recording sites. (a) Newly breaking wave. Here a ''plunging'' wave is depicted in the early stages of breaking, showing a classic jet curling over to fall against the face of the wave. In ''spilling'' waves, well-defined jets are not present; instead wave crests spill over (without creating an open air-filled tube) to form ''rollers'' that run down the wave face. (b) Fully breaking wave, produced after the jet or roller has subsequently injected disorganized flows into the base of the wave.

had injected large-scale eddies throughout the wave face, initiating overall degeneration of the waveform and energetic, disorganized water motion even in the wave base, were placed in a second classification termed ''*fully breaking*'' (Fig. 5b).

3.5.3. Water acceleration versus inshore wave height

Water accelerations produced by both newly breaking and fully breaking waves were examined as a function of inshore wave height at each of the four sites.

3.5.4. Simultaneous values of velocity and acceleration

The occurrence rate for encountering a given velocity at the same instant as a given acceleration was estimated as a function of wave height and relative orientation of the velocity and acceleration vectors. This information was generated as follows. Waves

from all sites in each of the newly breaking and fully breaking classifications were divided into several wave size classes, each class spanning a 0.5 m range in H. The velocity and acceleration pairs at every time point during the passage of a wave of a given size class were placed into a two-dimensional array composed of multiple 1 m/s and 10 m/s^2 velocity–acceleration bins, for each of four categories of relative vector orientation (velocity and acceleration acting along lines within 44°, 45 to 89°, 90 to 134°, and 135 to 180° of one another). It was noted whether the simultaneous velocity-acceleration pair corresponding to each bin occurred (or not) during a wave, and the total number of occurrences across all the waves in a given wave size class/orientation category was computed. The number of occurrences divided by the number of waves from each size class/orientation category yielded the fraction of waves of a given category that produced a particular velocity and acceleration pair simultaneously at least once during a wave's passage.

4. Results

4.1. Wave height distributions

Table 2 lists the rms wave heights, dominant wave periods, and tidal heights from each of the 28 measurement sessions. Surf-zone H_{rms} values across these sessions ranged from 0.31 to 1.26 m, spanning sea conditions of relative calm to storm swell. Deep-water H_{rms} values are given for sessions where measurements with the subtidal wave gauge were made simultaneously with the intertidal recordings. The largest deep-water rms wave height recorded was 1.03 m, corresponding to a significant wave height (H_s, a standard oceanographic measure defined as the average height of the highest 1/3 waves, roughly calculated as $\sqrt{2}\ H_{rms}$) of approximately 1.45 m (H_s was also likely greater during session 21, but there are no subtidal data for this date). Although such H_s values are not large for waters of the open coast, they are characteristic of the level of wave action produced within Monterey Bay as a consequence of moderately severe winter storms. For example, the mean monthly maximum significant wave height recorded during the winter months of 1991 at a location 300 m away from the subtidal site used in these experiments was 1.63 m (J. Watanabe, unpublished data).

Surf-zone wave height distributions fell into two basic categories. Distributions in the first group were characterized by a Rayleigh shape, consistent with extant data from gently sloping sandy beaches (Thornton and Guza, 1983). Distributions in the second category, however, possessed a symmetrical shape more reminiscent of a Gaussian process. Representative examples of these two types of distributions are shown in Fig. 6, and possible reasons for the deviation of the second type from the Rayleigh form are explored in the Discussion. In general, the symmetrical-type distributions were more common; site 2 was the only location that consistently showed wave height distributions having a Rayleigh appearance. The single exception to this rule occurred during one recording session at site 3 where the waves were much smaller than those of any of the other sessions. The mean and variance of H from the symmetrical wave height

Table 2
Wave heights during the field recordings

Recording Session	Site	Tide (m)	Period (s)	Surf zone					Deep-water	
				H_{rms} (m)	Mean (m)	σ^2 (m^2)	Shape[a]	Type[a]	H_{rms} (m)	H_s (m)
1	1	+1.10	12	0.71	0.68	0.041	S	FB	–	–
2	1	+1.21	11	0.76	0.74	0.029	S	FB	–	–
3	1	+1.08	–	–	–	–	–	–	0.83	1.17
4	1	+1.16	10	1.01	0.98	0.057	S	FB	0.83	1.17
5	1	+1.24	11	0.90	0.87	0.046	S	FB	0.74	1.04
6	1	+1.44	11	0.93	0.91	0.043	S	FB	0.76	1.07
7	1	+1.44	11	1.11	1.09	0.056	S	FB	1.03	1.45
8	2	+1.30	11,18	1.22	1.03	0.458	R	NB	0.87	1.23
9	2	+1.65	10	0.92	0.80	0.170	R	NB	0.73	1.03
10	2	+0.69	10	0.67	0.53	0.169	R	NB	–	–
11	3	+0.46	10	0.31	0.27	0.024	R	FB	–	–
12	3	+1.31	10	0.71	0.66	0.061	S	FB	0.80	1.19
13	3	+1.59	10	0.81	0.79	0.044	S	FB	0.74	1.04
14	3	+1.33	10	0.71	0.69	0.029	S	FB	0.72	1.01
15	3	+1.55	10	0.74	0.71	0.043	S	FB	0.88	1.24
16	1	+1.54	13	0.78	0.77	0.024	S	NB	–	–
17	1	+1.21	14	0.98	0.95	0.061	S	NB	–	–
18	1	+1.31	13	0.93	0.91	0.030	S	NB	–	–
19	1	+1.82	–	–	–	–	–	–	–	–
20	1	+1.40	13	1.08	1.07	0.028	S	NB	–	–
21	1	+1.68	12	1.26	1.24	0.051	S	NB	–	–
22	4	+1.51	12	0.76	0.74	0.032	S	FB	–	–
23	4	+1.51	12	0.76	0.74	0.029	S	FB	–	–
24	1	+1.17	9	0.41	0.38	0.025	S	FB	–	–
25	1	+1.23	9,16	0.61	0.58	0.040	S	NB	–	–
26	1	+1.29	16	0.69	0.66	0.046	S	NB	–	–
27	1	+0.94	17	0.55	0.50	0.043	S	NB	–	–
28	1	+0.98	8	0.52	0.48	0.036	S	FB/NB	–	–

[a] Surf-zone parameters were not computed for sessions 3 and 19 due to the smaller numbers of waves recorded during these tides. Shape refers to either Rayleigh-form (R) or symmetrical-form (S) surf-zone wave height distributions, and the type of wave breaking is categorized visually either as fully breaking (FB) or newly breaking (NB).

distributions are also listed in Table 2, since H_{rms} no longer acts as an effective single descriptor for these non-Rayleigh probability density curves.

4.2. Surf-zone velocities

A characteristic velocity trace is shown in Fig. 7a (along with the accompanying acceleration and wave height data in panels b and c for comparison), and serves to point out several general features of the intertidal water velocities recorded in this study. First, measured velocities were often large, routinely exceeding 5 m/s. These values are of similar magnitude to those measured by Koehl (1982, 1984) and Denny (1985) at

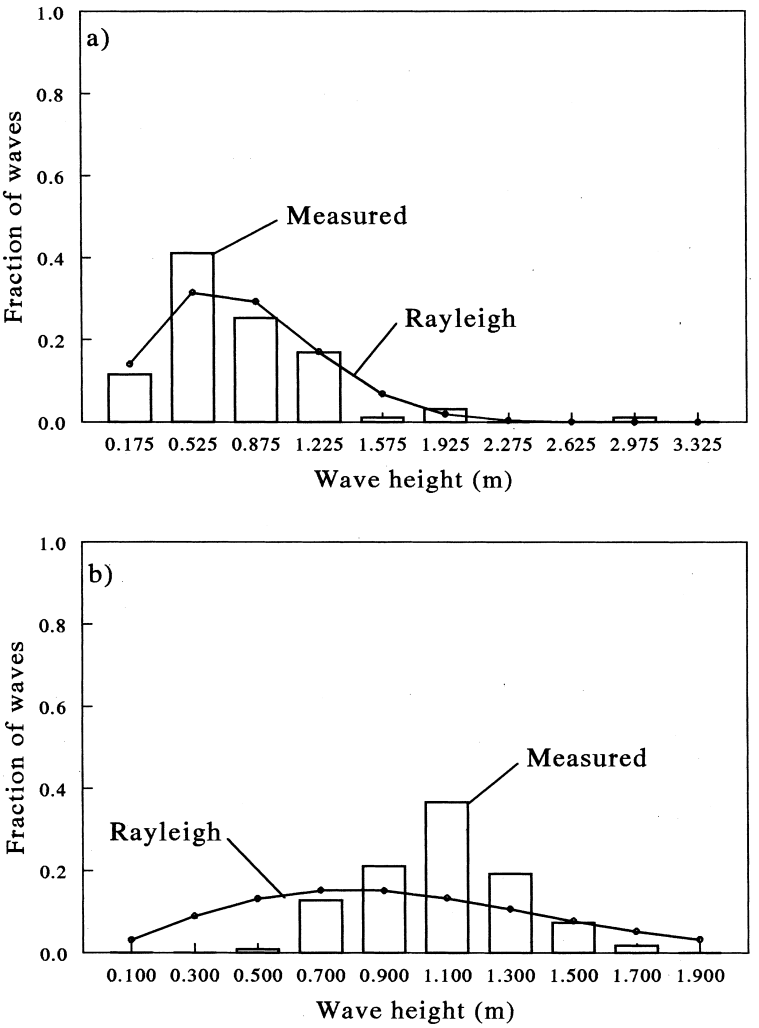

Fig. 6. Representative examples of inshore wave height distributions. The Rayleigh distributions corresponding to the same H_{rms} are shown in each panel for comparison. (a) Typical Rayleigh form. (b) Typical symmetrical form.

Tatoosh Island off the coast of Washington state. Second, alongshore components of velocity near the substratum were often of similar magnitude as (or even greater than) the seaward-shoreward components. This feature was also noted by Koehl (1977) and Denny (1985), and most likely follows from the wave reflection, redirection, and channeling which occurs as waves propagate across uneven substrata. Third, the level of variation in velocity through a wave was often substantial, particularly during the early phases of wave breaking when large-scale energetic flows associated with the plunging crest still dominated. Later during wave passage, presumably after much of the energy

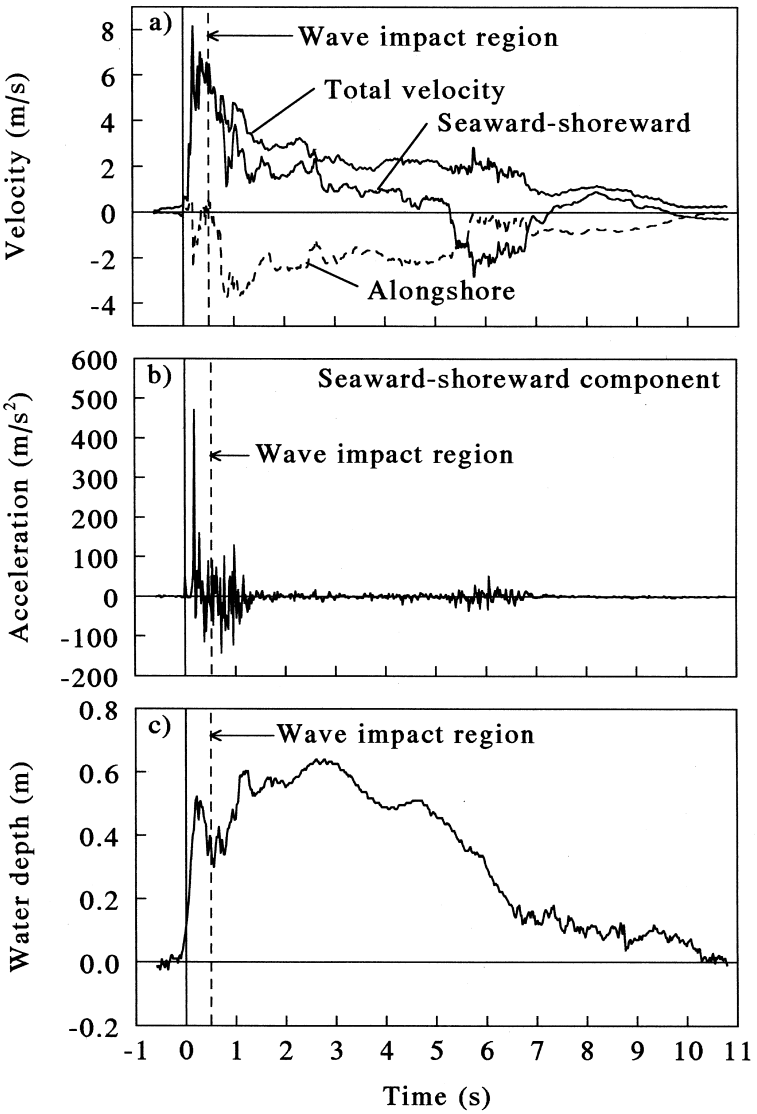

Fig. 7. Characteristic flow traces from a single wave in the field. (a) Shoreward-seaward and alongshore components of velocity, as well as their vector sum. (b) Shoreward-seaward component of acceleration. (c) Water depth showing the passage of the wave. Note that during the initial 0.5 s after a wave's arrival, impact-type forces occur which can potentially bias flow estimates (see, for example, the spike in panel b). As a consequence, flow estimates from the first 0.5 s are excluded from subsequent analyses.

associated with these large-scale motions had been transferred to smaller-sized eddies, velocity profiles became more uniform through time.

Larger waves produced larger velocities, but the exact nature of this relationship depended critically on details of wave breaking. A primary factor determining the

character of the u–H relationship was the type of breaking (i.e., newly or fully breaking). Fig. 8a shows how the maximum velocities from each wave, u_{max}, varied with intertidal wave height for newly breaking waves pooled from multiple recording sessions and sites. Under newly breaking conditions, maximum velocities recorded near the substratum by the probes were remarkably well represented by the empirical bore approximation of Eq. 3. That is, velocities increased as $u_{max}=\sqrt{gH}$. All of the recording sessions at site 2 and many at site 1 were characterized by newly breaking waves. In contrast, fully breaking waves produced maximum velocities that often differed substantially from values predicted by the empirical bore approximation, increasing at a faster rate with wave height than a $H^{1/2}$ proportionality. Fig. 8b shows these data pooled from multiple recording sessions at sites 1, 3 and 4. The largest maximum velocities, one particular measurement reaching nearly 11 m/s, were recorded under fully breaking waves. Such extreme values are roughly in accordance with previous estimates made from multiple-day deployments of maximum-force recording spring scales (Jones and

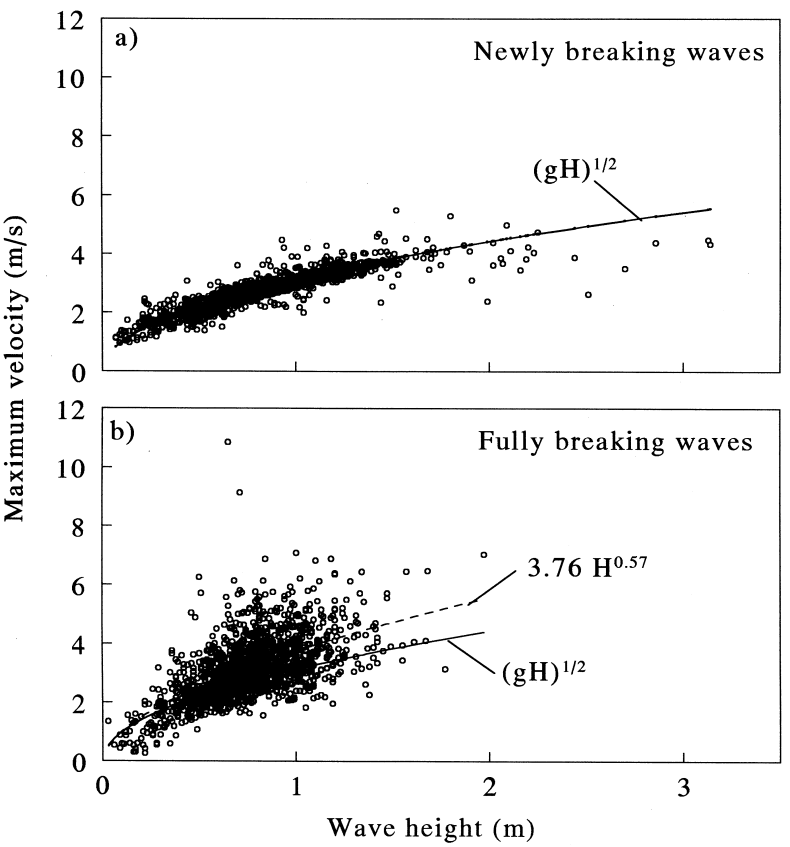

Fig. 8. Maximum water velocities produced by (a) newly or (b) fully breaking waves. Note that maximum velocities under fully breaking waves are not well predicted by the theoretical $(gH)^{1/2}$ function; the empirical fit is shown for comparison.

Demetropoulos, 1968; Bell and Denny, 1994), although the exact sizes of the waves corresponding to the velocity estimates of these authors are unknown.

The scatter apparent in the overall u_{max}–H relationships of Fig. 8a and 8b arose from multiple sources. Maximum velocities showed not only variation on a wave by wave level, but also on a day by day and site by site basis. These features became apparent once the underlying trend of increasing maximum velocity with increasing H was removed, a step accomplished by normalizing the u_{max} values by $\sqrt{gH}$ for the newly breaking waves and by the empirical power curve fit to the u_{max}–H data for the fully breaking waves ($u_{max} = 3.76\ H^{0.57}$, $r^2 = 0.37$). Day by day differences are shown in Fig. 9, where normalized maximum velocity distributions from three representative recording sessions with either newly or fully breaking waves are graphed for site 1. Comparison of the two panels in Fig. 9 indicates that both the differences from day to day as well as the within-day variance in normalized maximum velocity are lower under newly breaking

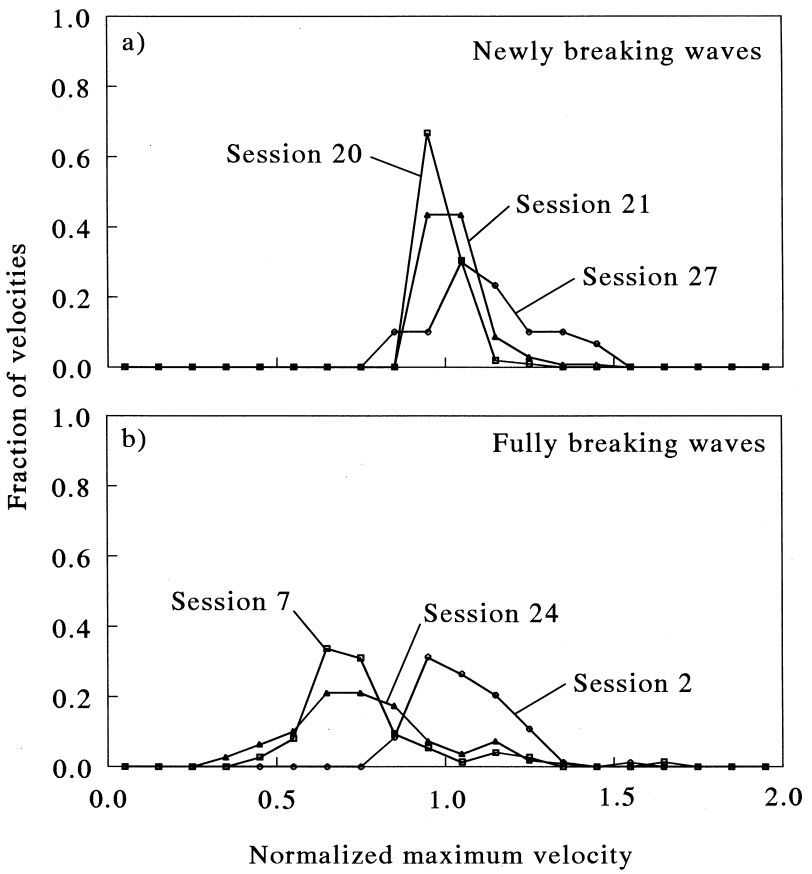

Fig. 9. Representative maximum velocity frequency polygons from three recording sessions with (a) newly or (b) fully breaking waves. Velocities are normalized by $(gH)^{1/2}$ in (a) and by the empirical fit to the values of Fig. 8b in (b) to remove effects of wave height. Data were recorded at Site 1.

than fully breaking waves, as would be expected from reference to Fig. 8. The normalized maximum velocity distributions are also less skewed under newly breaking than fully breaking waves. Analogous between-site differences in normalized maximum velocity distributions for either newly or fully breaking waves are presented in Fig. 10, where each curve is composed of the pooled data from all the recording sessions made at a single site during waves of a given breaker type. Note that the level of variation between sites is similar to the between-day variation within a site. Also note that in general the shapes of the distributions are sufficiently skewed and variable (as well as being composed of enough points to yield substantial statistical power) to routinely violate both conditions of normality and homogeneity of variance. Although this feature precludes the use of many of the standard parametric statistical tests for examining the significance of between-day/site differences in distribution means, it also makes such tests unnecessary since substantial variability in the shape of the underlying distributions indicates that the details of the physical processes responsible for producing surf-zone

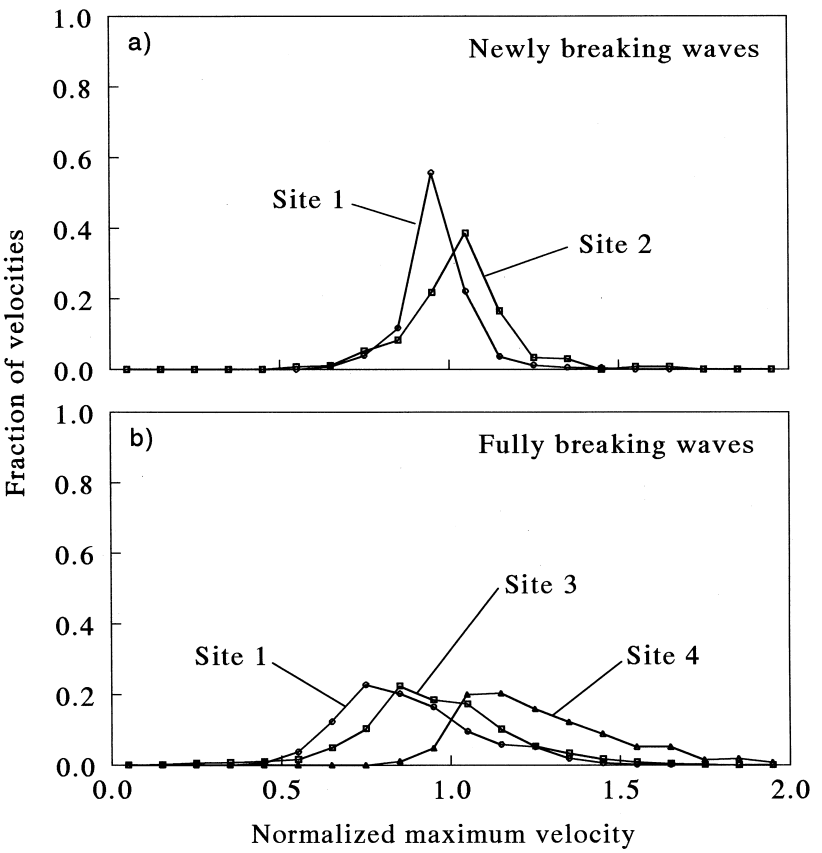

Fig. 10. Maximum velocity frequency polygons from each field site. Curves are composed of pooled data from all recording sessions at a given location, for either (a) newly or (b) fully breaking waves. Velocities are normalized as in Fig. 9.

velocities indeed differ through time and space. Implications of this result are explored in further depth in the Discussion.

In summary, the surf-zone velocities recorded in this study were characteristically large and varied substantially in magnitude and direction. Maximum velocities under newly breaking waves tracked closely the empirical $\sqrt{gH}$ relationship of Eq. 3, while those produced by fully breaking waves tended to be larger for a given wave height. For both newly and fully breaking waves, there was considerable variation in the maximum velocity produced by waves of a given size, both in time and space.

4.3. Surf-zone accelerations

A characteristic water acceleration trace is shown in Fig. 7b. The values apparent in this wave were not unusual, and much larger accelerations (several in excess of 400 m/s^2) were recorded during the course of the field measurements presented here. Both the direction and magnitude of the recorded accelerations changed rapidly, on time scales much shorter than those that characterized the velocity fluctuations. Also, the coefficient of variation was typically quite large.

As with surf-zone velocity, the maximum water acceleration produced by a breaking wave typically increased with wave height, although this trend was weak and contained substantial variability. Fig. 11a shows the maximum acceleration versus wave height relationship for newly breaking waves, and Fig. 11b shows the corresponding relationship for fully breaking waves. In general, larger maximum accelerations occurred under fully breaking waves of a given height than under newly breaking waves of the same height. For rough comparative purposes, a simple linear regression was fit through the newly breaking data, and yields $(du/dt)_{max} = 38.56\ H + 15.26,\ r^2 = 0.16$. In contrast, maximum accelerations produced by fully breaking waves increased much more rapidly with wave height (the linear regression fit through the lumped fully breaking data is $(du/dt)_{max} = 114.13\ \ H - 1.49,\ \ r^2 = 0.22$). Note, however, that due to violation of assumptions of homogeneity of variance, these linear regressions provide only approximate rather than precise descriptors of the relationship of maximum acceleration to wave height (transformed regressions were also inappropriate due to non-monotonic changes in variance across H). Thus too much emphasis should not be placed on the exact slopes of the above fits.

The above regressions do, however, provide a crude means of normalizing the accelerations to remove the effect of the covariate, H. This procedure demonstrates that normalized maximum acceleration, like normalized maximum velocity, contained both within-wave as well as between-day/site variability. Between-day (Fig. 12) and between-site (Fig. 13) differences in the normalized maximum acceleration distributions were observed for both newly and fully breaking waves. The normalized maximum acceleration distributions were also substantially more skewed to the right than the corresponding velocity distributions, suggesting that there was not a sharp and stringent upper bound on acceleration magnitude.

Together the above data indicate that exceptionally large accelerations occur in surf-zone flows, and that the magnitudes of accelerations vary markedly through a given wave cycle at time scales substantially shorter than the analogous variations in velocity.

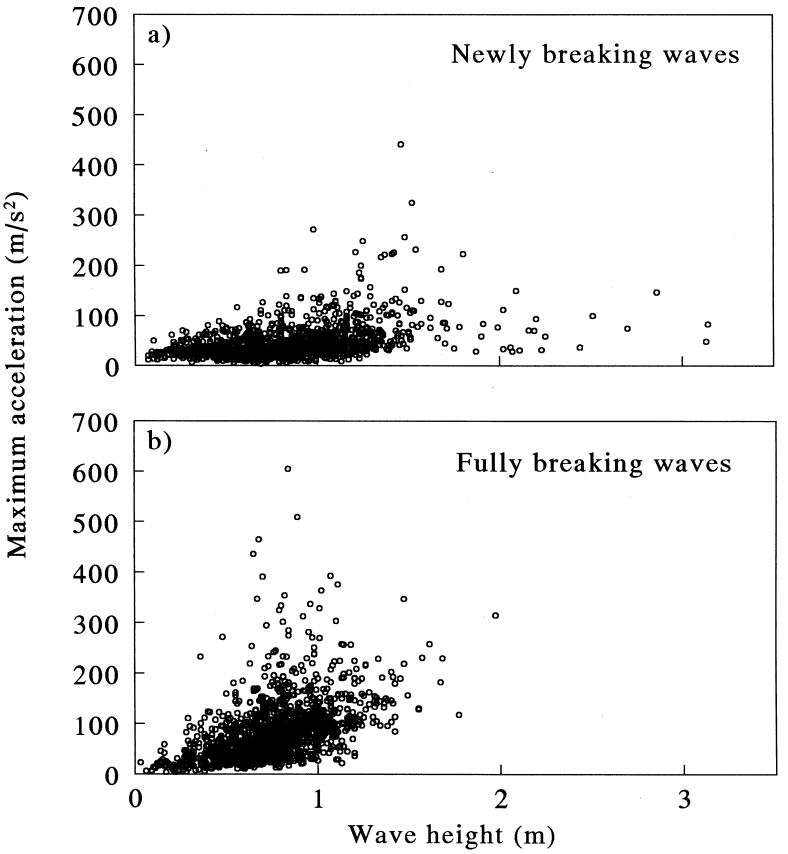

Fig. 11. Maximum water accelerations produced by (a) newly or (b) fully breaking waves.

Maximum accelerations also varied from day to day and among locations, and were often larger for a given wave height under fully (as compared to newly) breaking waves.

4.4. Simultaneous velocity and acceleration

Instantaneous values of co-occurring velocity and acceleration in a single representative wave are plotted in Fig. 14, demonstrating the absence of any strong relationship between simultaneous velocity and acceleration magnitude. The substantial scatter apparent in this graph suggests that although the magnitudes of the two quantities are not completely independent (i.e., Eulerian acceleration is the total derivative of velocity), any relationship between their concurrent values can only be described statistically.

Fractional rates of co-occurrence of velocity and acceleration, for several ranges of H and for both types of wave breaking, are shown in Figs. 15 and 16. These data apply to the subset of measurements where the angular separation of the velocity and acceleration vectors was less than 45°. The occurrence rates presented in these plots reflect the

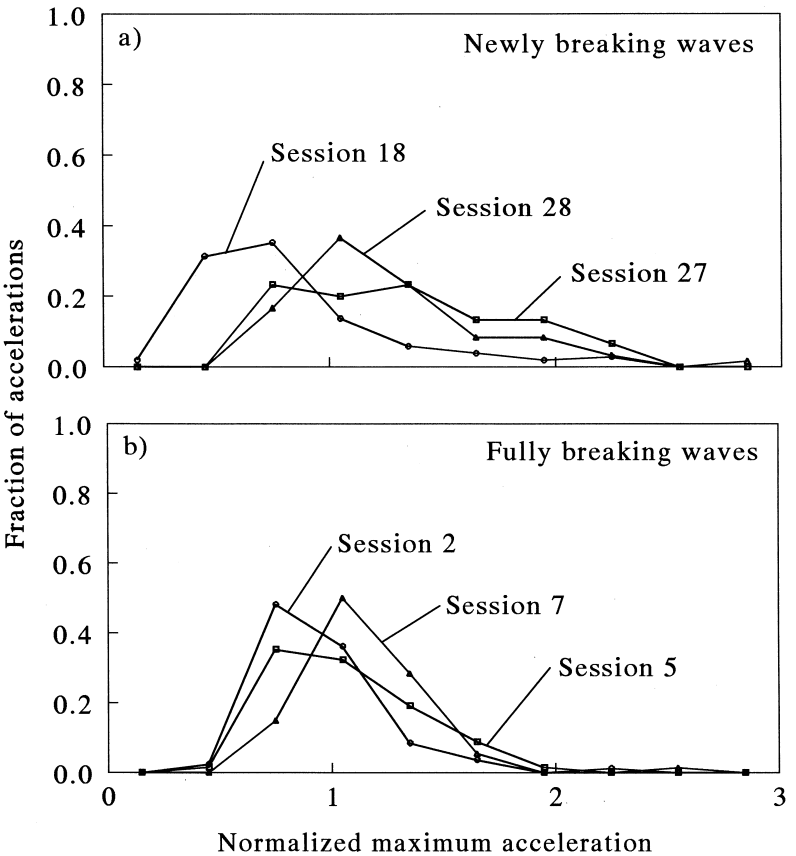

Fig. 12. Representative maximum acceleration frequency polygons from three recording sessions with (a) newly or (b) fully breaking waves. Accelerations are normalized by empirical fits to the values of Fig. 11a and b (see text) in (a) and (b), respectively, to remove effects of wave height. Data were recorded at Site 1.

fraction of waves of a given breaker type that produced particular flow conditions at least once during a wave's passage. Figs. 15 and 16 show that small waves typically produced smaller co-occurring velocities and accelerations than those generated by larger waves. For example, fully breaking waves 0–0.5 m high produced 1.5 m/s velocities and 25 m/s^2 accelerations approximately 50% of the time (Fig. 16a), while 1.0–1.5 m high waves breaking in a similar fashion generated 3.5 m/s and 70 m/s^2 velocities and accelerations with equal regularity (Fig. 16c). Note that 1.0–1.5 m high waves (which occurred quite routinely) produced simultaneous velocities and accelerations in excess of 5 m/s and 150 m/s^2, respectively, about 5% of the time. Flows of this magnitude can be found in few environments other than the intertidal zone.

Differences in simultaneous velocity-acceleration occurrence rates existed between the two types of breaking waves. For a given size wave, newly breaking waves were less likely to produce co-occurring velocities and accelerations of large magnitude than fully

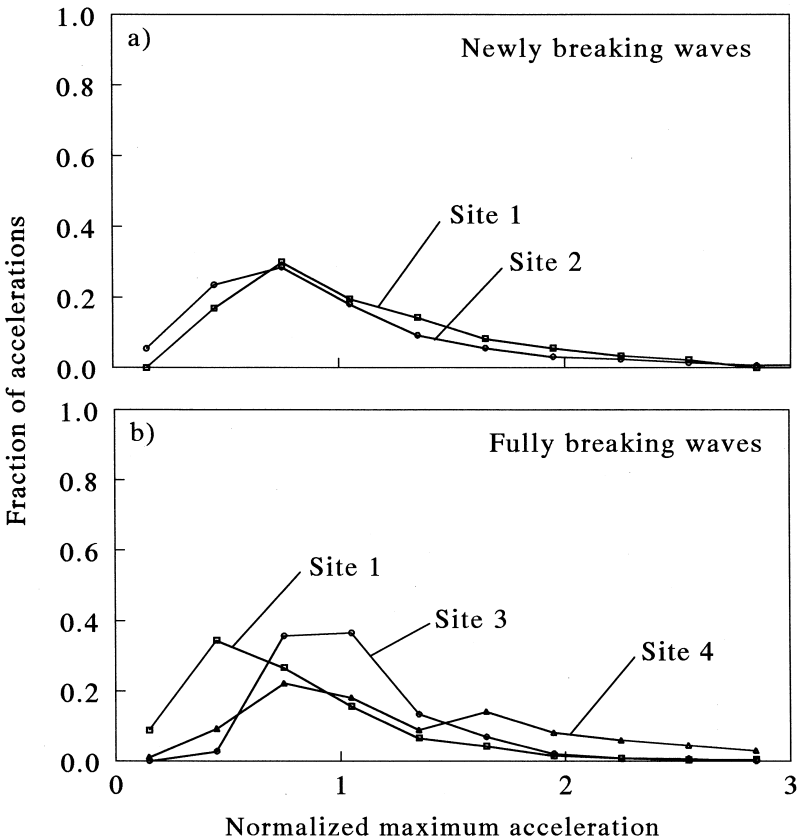

Fig. 13. Maximum acceleration frequency polygons from each field site. Curves are composed of pooled data from all recording sessions at a given location, for either (a) newly or (b) fully breaking waves. Accelerations are normalized as in Fig. 12.

breaking waves (compare matching panels in Figs. 15 and 16). For example, 4 m/s velocities in conjunction with 100 m/s^2 accelerations occurred in 20% of 1.0–1.5 m high fully breaking waves (Fig. 16c), but were produced by fewer than 5% of newly breaking waves of the same size (Fig. 15c). Note that the largest wave height range shown for newly breaking waves is $1.5 < H \leq 2.0$ m (Fig. 15d), while the largest size class shown for fully breaking waves is $1.0 < H \leq 1.5$ m due to insufficient numbers of larger waves of this breaker type.

Although rate-of-occurrence graphs of simultaneous velocity and acceleration as a function of wave height are shown here only for a single orientation category (angular separation of the vectors less than 45°), the corresponding plots for 45–89, 90–134, and 135–180° are almost identical. This consistency can be seen in Fig. 17 (compare to Fig. 16b), where contour plots from the remaining three angular categories of fully breaking waves of intermediate size ($0.5 < H \leq 1.0$ m) are presented.

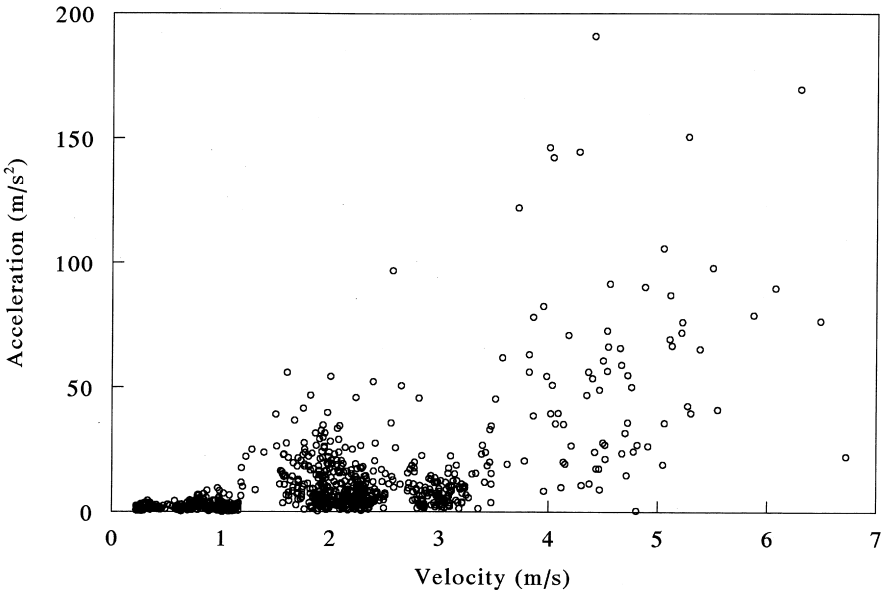

Fig. 14. Simultaneous velocities and accelerations during a single fully breaking wave recorded at site 4.

5. Discussion

5.1. Wave height distributions

Recently, Denny (1995) has developed a mechanistic theory for quantifying exposure and predicting disturbance rates of intertidal organisms. This approach relies on the assumption of Rayleigh-distributed deep-water and inshore wave heights. However, although the Rayleigh character of offshore wave height distributions is well documented, it has remained unclear whether the shapes of these incident deep-water distributions might be modified when waves move inshore and break (e.g., see Hughes and Borgman, 1987), particularly at locations where shorelines are steep, rocky, and irregular. Here we explore in more detail the results of this study which suggest that wave height distributions in the surf zone may differ from those a short distance offshore.

Previous measurements by Thornton and Guza (1983) indicate that the heights of waves at given depths in the surf zone of gently sloping sandy beaches can be approximated by Rayleigh distributions specified by local H_{rms} values. The wave height distributions of the breaking waves forming subsets of these overall distributions were fit empirically by applying a weighting function to each total Rayleigh probability density curve. The empirical breaking wave distributions (one at each depth) exhibited more symmetrical shapes, with fewer small waves than would be predicted by a Rayleigh distribution. Such a deficit of smaller waves likely arises as a consequence of the tendency for waves of lesser height to break inshore of larger waves. Because the

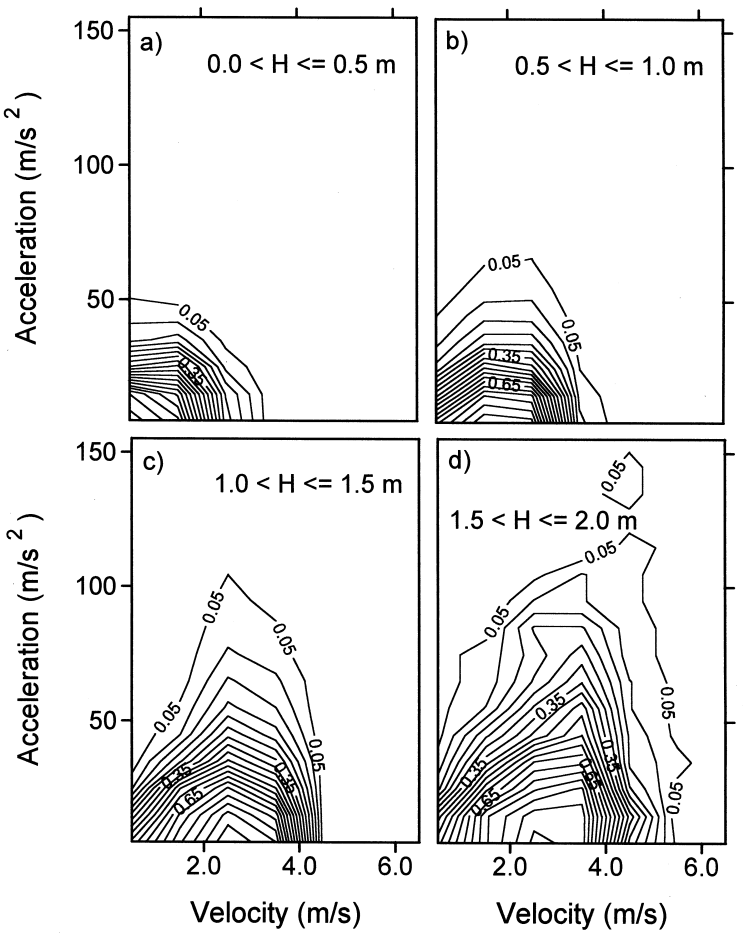

Fig. 15. Fractional joint rates of occurrence of velocity and acceleration under newly breaking waves. Contours show the fraction of waves that produced simultaneous velocities and accelerations of given magnitude that also acted within less than 45° of the same direction, for four wave height ranges. (a) Waves less than or equal to 0.5 m in height. (b) Waves greater than 0.5 m up to 1.0 m in height. (c) Waves greater than 1.0 m up to 1.5 m in height. (d) Waves greater than 1.5 m up to 2.0 m in height.

smallest waves propagating past a particular location in a surf zone may not break there, they tend to be excluded from any breaking wave height distribution calculated for that depth. In contrast, the largest waves impinging on a shore tend to break offshore of a particular location in a surf zone, resulting in a truncation of the large-wave tail of a given depth's wave height distribution. These two factors together tend to drive the shape of a breaking wave height distribution away from a Rayleigh curve towards a more symmetrical form.

If such processes continue to the limiting case of exceptionally shallow water (where essentially all waves are breaking), and if the same phenomena occur on steep shores,

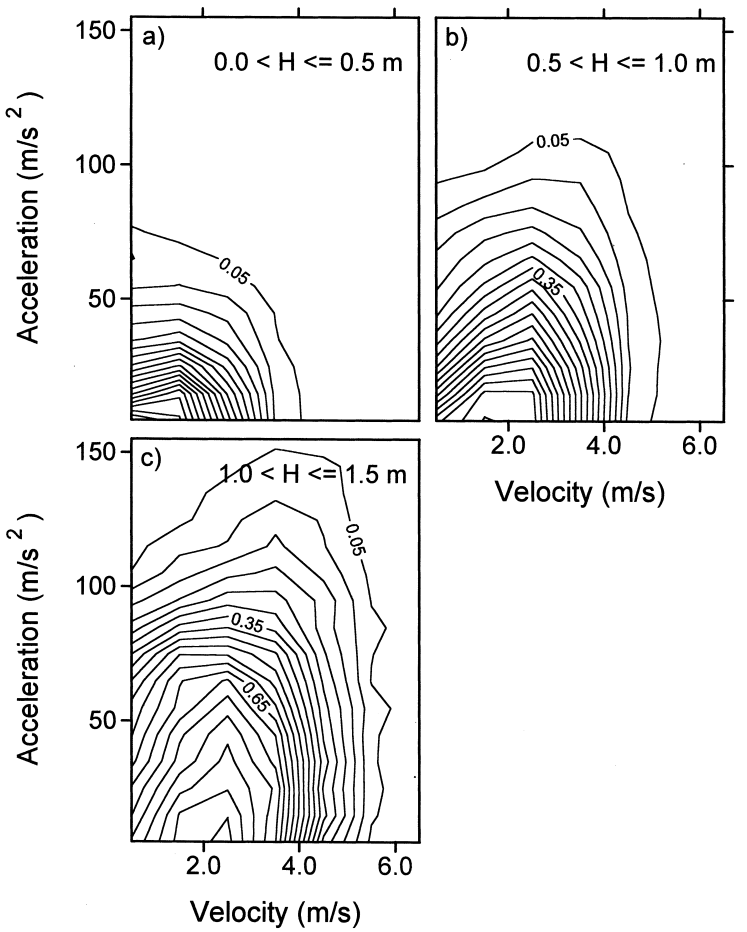

Fig. 16. Fractional joint rates of occurrence of velocity and acceleration under fully breaking waves. Contours show the fraction of waves that produced simultaneous velocities and accelerations of given magnitude that also acted within less than 45° of the same direction, for three wave height ranges. (a) Waves less than or equal to 0.5 m in height. (b) Waves greater than 0.5 m up to 1.0 m in height. (c) Waves greater than 1.0 m up to 1.5 m in height.

they might explain the non-Rayleigh form of the wave height distributions observed in the present study at sites 1, 3, and 4. Alternatively, there may be an analogous physical ''filtering'' effect that operates on rocky shores with highly irregular topography. The manner in which this second possibility might arise is as follows.

The topography of rocky coasts is in general composed of exceptionally uneven substrata. The way in which topographical features interact with a wave depends on its size. Large waves are more apt than small waves to experience substratum complexity as effective roughness elements (albeit impressively large ones) rather than as a series of imposing obstacles. A minor benthic protrusion to a large wave may act as an impassible

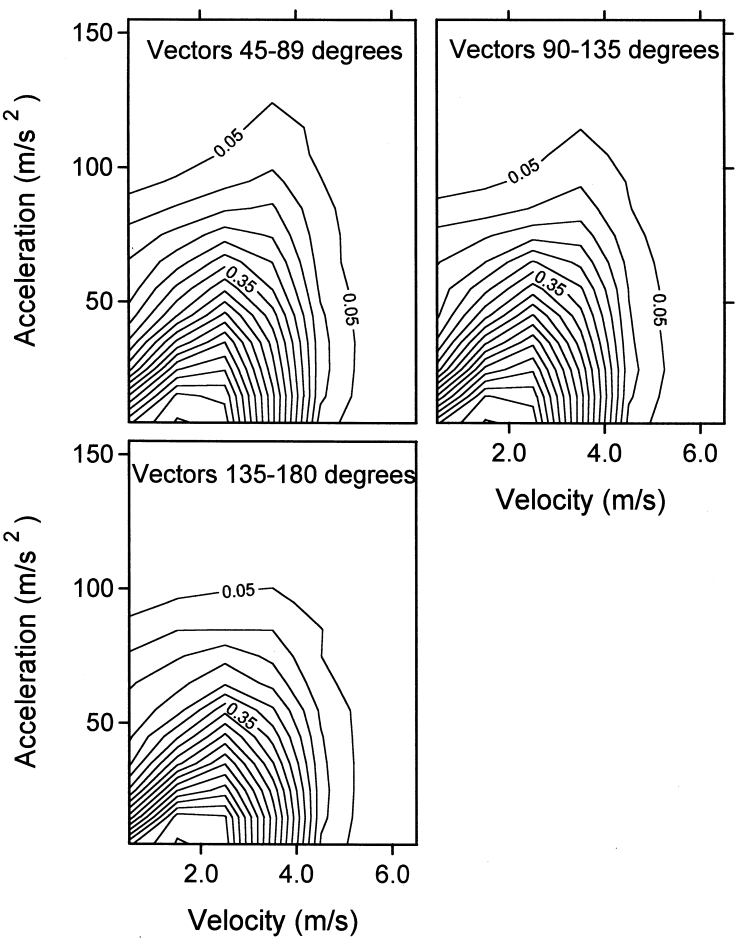

Fig. 17. Fractional joint rates of occurrence of velocity and acceleration under fully breaking waves of the 0.5 to 1.0 m size class, for three categories of relative vector orientation of velocity and acceleration. (a) Angular deviation between velocity and acceleration vectors of 45–89°. (b) Angular deviation 90–134°. (d) Angular deviation 135–180°.

barrier to a smaller wave, causing reflection, redirection, rapid dissipation of energy, and preventing its further progress up the shore. Thus there may be a tendency for small waves on rocky coasts to be eliminated from a wave height distribution measured substantially shoreward of the mean break point. The powerful backwash of large waves on steep shores may also obliterate smaller bores before they can move into the swash zone. These two factors may act synergistically to explain the relative lack of small waves, compared to a Rayleigh curve, observed in the wave height distributions at sites 1, 3, and 4 of the present study.

In contrast to the other field sites, the sharp step that characterizes the topography of site 2 causes both large and small waves to break at the same location. Thus at this site

small waves do not in general propagate through intermediate-depth regions where backwash from larger waves might disrupt their travel towards a shallower breaking point. Furthermore, the recording location at site 2 is positioned within 0.5 m of the edge of the step, so there are no auxiliary obstacles of varying spatial scale to disproportionately obstruct and dissipate smaller waves. These features of site 2 may minimize any potential for modification of the impinging deep-water Rayleigh distribution.

5.2. Wave period, tidal height, and the type of breaking

Figs. 8 and 11 show clearly that different physical processes operate near the substratum under newly breaking waves than fully breaking waves. Under newly breaking waves, maximal water velocities at the height of the probes (2 cm) appear to equal the near-substratum bulk velocity associated with the propagating waveform (approximately $\sqrt{gH}$). This is presumably because the large-scale eddies produced in the initial phases of wave breaking have not yet invaded the lower part of the wave; therefore the only major fluid motion relative to the probes is that associated with the overall movement of the bore. This is in contrast to the variation of maximum velocity with wave height under fully breaking waves where little more than a general trend exists between u_{max} and H. The increase in variability under fully breaking waves is likely due to the superposition of energetic large-scale fluid motion associated with breaking onto the bulk velocity associated with the phase speed of the waveform. Such breaking phenomena may also explain the deviation of the fully breaking u_{max}–H relationship away from a square root function (Fig. 8b). Because there is greater variability in velocity under larger waves, and because maximum values reflect peak excursions away from an underlying process characterized by increasing variance with increasing H, velocity maxima tend to exceed mean velocities by a greater margin as wave height increases. This tends to elevate the exponent in the empirical u_{max}–H power curve.

In much the same way, processes associated with wave breaking may also lead to the observed variability in maximum acceleration as a function of wave height. This follows from the close link between fluid accelerations (generated by advection of eddies past the probes) and the action of wave breaking which produces such eddies. The larger accelerations of fully breaking waves (Fig. 11) conceivably results from greater stochastic fluid motion at the elevation of the flow probes under fully as compared to newly breaking waves. Note, however, that the observed differences in near-bottom flows between newly and fully breaking waves are unlikely to hold for regions near the crests of waves where breaking processes in both breaker types are probably quite similar.

Because newly breaking waves evolve into fully breaking waves as they move inshore, plants and animals living somewhat higher in the intertidal zone may experience predominantly fully breaking waves, whereas those living lower may encounter mostly newly breaking waves. Such trends, however, are modulated by tidal height and the period of the waves. Thus, an organism subjected to newly breaking waves of a given deep-water wave height at high tide may experience waves of the same deep-water height as fully breaking when the tide falls to a lower level. This is analogous to Koehl's

(1982) observation that organisms exceptionally low in the intertidal zone may encounter unbroken waves at high tide but breaking waves at low tide. Similarly, because longer period waves of a particular H/d ratio can shoal farther inshore before breaking, an organism at a given location can encounter either fully or newly breaking waves of a particular height depending on the period of the waves. Effects such as these can be seen in data from the present study where most of the newly breaking waves at site 1 were recorded during conditions of smaller H_{rms} values relative to tidal height and/or waves of somewhat longer period. In contrast, fully breaking waves were present at site 1 when wave heights were larger relative to tidal height, and when wave periods were shorter. Denny (1985) also notes effects of tidal height in an explicit examination of such issues.

5.3. Intersite variability and generality of the measurements

Given the importance of water depth on wave shoaling, refraction, and breaking, details of substratum topography become critical factors determining the nature of intertidal water motion. Indeed, as has been emphasized by Koehl (1982, 1984), Denny et al. (1985), and Denny (1987) the contour variability characteristic of rocky coasts means that typical flows at one location may be substantially different from those occurring just centimeters away. For example one would expect much greater water velocities on the seaward apex of a protruding boulder than in a crevice located immediately behind it. For an organism small enough to live in either of these two locations, the relative differences in survivorship or food delivery between these sites could be immense. In contrast, for a much larger organism that spans these two regions, the more relevant hydrodynamic factor may be what the average water motion is like over a much larger area. Such issues indicate that spatial scales (both that of the organism as well as that of the site at which it lives) are critical parameters in defining a flow environment. These spatial scales then must be considered relative to the spatial scales of the waves themselves (i.e., wave height and to a lesser degree wavelength).

The length scales of wave height are relatively limited, falling in the range of a fraction of a meter to a few meters. In contrast, the sizes of intertidal organisms vary over a much broader spectrum (from smaller than millimeters to meters), while the scales associated with site topography include lengths spanning millimeters (e.g., roughness elements) to kilometers (e.g., headlands versus embayments). Clearly, describing the relationship between the flows occurring in the immediate vicinity of a particular organism and the general level of exposure characteristic of a 1 km stretch of coastline is impossible. However, the most complicated interactions between waves and topography occur at the length scales of the waves themselves. Water motion in cm-scale microhabitats can be modeled using existing fluid-dynamical theories (i.e., boundary layer or turbulence analogies) or empirical relationships from field and flume experiments once the local ‘‘mean flow’’ has been defined (Nowell and Jumars, 1984). Similarly, large-scale effects such as the increase in levels of wave action on headlands are well explained by existing wave refraction and shoaling analyses (U.S. Army Corps of Engineers, 1984). Thus the challenge for ecologists is to define the relationship between wave-generated flows and topographical features at the scale of one to several

meters. A first look at these issues is provided by data from the present study. Three major points emerge.

First, a comparison of the frequency polygons of Fig. 10 shows clearly that differences in characteristic levels of flow can exist among sites. Analogous variability between sites has been documented previously by Bell and Denny (1994), and is not surprising. Indeed, relative differences in water velocity between prominent intertidal features such as tide pools and surge channels can often be discerned by eye. In other cases, detecting subtler levels of variability may require careful measurements. For example, although flows at site 4 resembled qualitatively those at the other sites, velocities and accelerations were actually larger on average for a given H than those at the other locations (Fig. 10). In hindsight, this most likely arose as a consequence of the deployment of probe 4 within a narrow channel that funneled incoming waves.

It must also be emphasized that the four sites used in this study, while substantially different topographically, in no way span the entire spectrum of possible contour variation. For example, all of the sites chosen are positioned in regions lacking large obstructions within approximately a 1 m radius of the flow probes. Thus no measurements were conducted either in front of or on the lee sides of boulders or rock protrusions, or within crevices. Likewise, no measurements were conducted in surge channels or tide pools. Furthermore, velocity and acceleration magnitudes most likely vary with elevation on the shore. Sites high in the swash zone probably experience more benign water motion (primarily splash or low-energy run-up), while as noted above, mid- and low-intertidal regions likely encounter predominantly fully or newly breaking waves, respectively. Together these factors mean that a complete description of time-integrated topography effects would require measurements from an exceptionally large number of sites.

The second major point to emerge from the data is that there is substantial variation from day to day within a single site, even when wave height effects are removed (Figs. 9 and 12). The level of this variation rivals that occurring across sites (Figs. 10 and 13). Presumably such between-day differences in flow arise as a consequence of shifts in the direction of the incoming swell, changes in the wave spectrum (e.g., the dominant period, narrow-banded versus wide banded), as well as differing tidal height and perhaps wind strength/direction. Such interactions indicate that topography effects are not stand-alone quantities; it is the interplay between varying sea conditions and topography that determines the flow at a particular location and time.

This point leads to the third conclusion that can be drawn from this study. Although the measurements described here include high frequency recordings from over 2700 individual waves impinging on four sites during a variety of sea states, they in no way provide a complete description of surf-zone water motion on rocky coasts. Such a task is clearly formidable. Nonetheless, the measurements made here do provide a basic framework for constructing an improved picture of what the highly variable and complex fluid velocities and accelerations in the intertidal zone can be like. In particular, these measurements yield both a quantitative description of simultaneous values of velocity and acceleration, as well as a first empirical look at their relationship to the heights of waves impinging on steep rocky substrata. In practice, therefore, these data can be used as a set of fine-scale measurements against which coarser, time-integrated indices of flow can be juxtaposed.

5.4. Intertidal versus subtidal flows

Viewed as high-resolution snapshots, the flow data are especially useful for reemphasizing the marked hydrodynamic differences between intertidal and subtidal habitats, differences that may have important ecological consequences for the plants and animals living in these environments. Five distinguishing features are outlined below.

5.4.1. Flow magnitudes

Subtidal flows are much slower than those in the surf zone. Using expressions from linear wave theory (Denny, 1988) it is possible to estimate the peak near-substratum velocities and water particle accelerations produced by waves outside the breaker region:

$$u_x = \frac{\pi H}{\tau}\frac{1}{\sinh(2\pi d/L)}, \quad \partial u_x/\partial t = \frac{2\pi^2 H}{\tau^2}\frac{1}{\sinh(2\pi d/L)}. \tag{9}$$

In these equations, τ is the wave period, L is wavelength (related to τ via the standard dispersion relation, see Pond and Pickard, 1983), and sinh indicates the hyperbolic sine function. Taking an extreme case, a 10 s period, 6 m high unbroken wave in 5 m of water (i.e., approximately the largest yearly wave one would expect at a moderately exposed location on the west coast of North America, at the shallowest depth limit for a non-breaking wave of this size (Denny, 1995)) produces horizontal velocities near the substratum of roughly 4.5 m/s and horizontal water accelerations of about 3 m/s^2. In comparison, reference to Figs. 8 and 11 shows that similar flow rates are produced by surf-zone breakers of quite mundane size (i.e., 1 m high). In general, velocities in the intertidal zone are 2 to 5 times larger than those found subtidally, while surf-zone accelerations may be greater by two orders of magnitude. Recalling that drag and lift vary with the square of relative water velocity, it is clear why there is a much greater potential for flow-induced damage and mortality in intertidal locations. Implications of the larger accelerations are less clear; this topic is discussed in further depth elsewhere (Gaylord, in prep.).

5.4.2. Flow directionality

Previously Koehl (1977) and Denny (1985) have shown that near-bottom intertidal flows are highly variable directionally. Although not explored in a detailed fashion here, results from the present study support this finding (e.g., see Fig. 7a). Thus, while the potential exists for subtidal plants and animals to reliably orient themselves to the bidirectional surge of nonbreaking waves or to currents, analogous behaviors would serve little purpose in the surf zone.

5.4.3. Time scales of flow

Another difference between intertidal and subtidal flows is the characteristic time periods over which velocities and accelerations vary. Subtidally, oscillations in velocity or acceleration occur regularly with frequencies of a fraction of a Hz. In contrast, intertidal velocities change on time scales that span frequencies from less than one to several Hz. A representative surf-zone velocity power spectrum (consult Bendat and Piersol (1986) for details on calculation methods) is presented in Fig. 18a, showing the

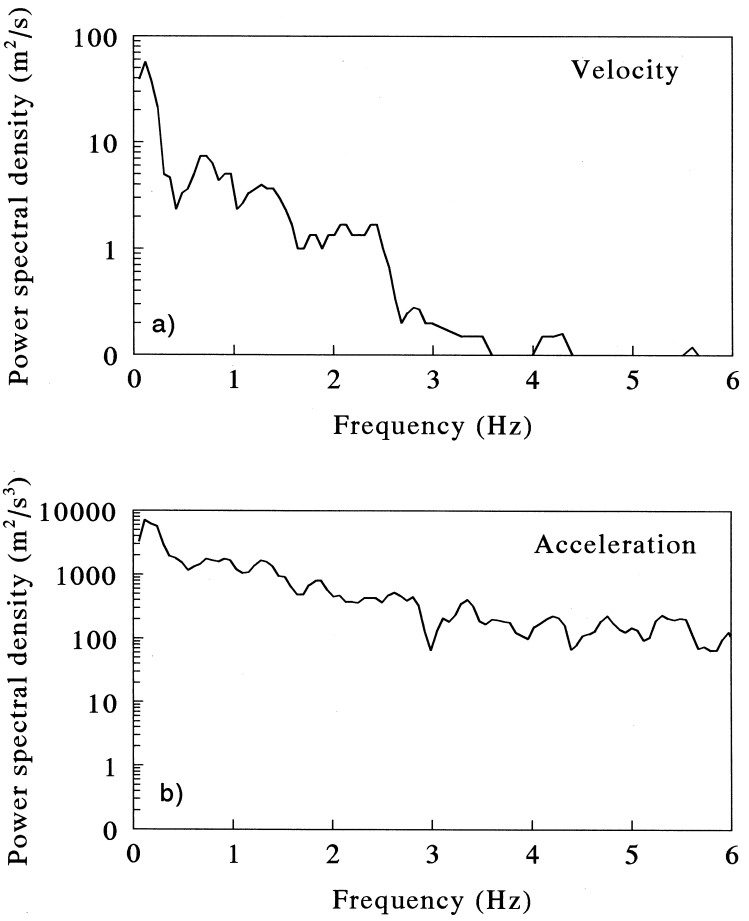

Fig. 18. Representative power spectra of (a) velocity and (b) acceleration under a fully breaking wave.

dominant frequencies of flow variability. Fig. 18a indicates that, in addition to the major oscillations occurring at the frequency of the overall waveform (responsible for the peak at 0.1 Hz, corresponding to 10 s period waves), there is also substantial velocity variation at frequencies up to 3 Hz. Similarly, a representative power spectrum of intertidal acceleration (Fig. 18b) also includes power smeared across a large range of frequencies. In particular note that the spectrum for acceleration still contains measurable power at the 6 Hz right-hand limit of Fig. 18b. Although not shown, this tail continues out into the 25–50 Hz range.

Such differences in temporal variability between subtidal and intertidal environments may be important in at least two biological contexts. First, the time course of applied loads can interact with the motion of flexible organisms to increase or decrease the forces they must endure. For example, Koehl (1982, 1984, 1986) notes that large subtidal seaweeds such as the giant kelp, *Macrocystis pyrifera*, may experience

decreased drag via a reduction in relative water velocity as the plants passively move with waves. Alternatively, once an attached organism begins to deflect, it develops momentum that may apply an inertial force when it is again forced to decelerate. Denny et al. (1998b) explore this issue through the use of several general models, showing that the frequency of the externally imposed force, relative to the preferred frequency of oscillation of an organism, is a critical factor determining the level of inertial force applied to a deformable plant or animal. Gaylord and Denny (1998) and Denny et al. (1998a) discuss this topic further. Because velocities and accelerations vary according to vastly different time scales intertidally as compared to subtidally, the consequences to an organism of hydrodynamic forces even of identical magnitude may differ substantially between the two environments. For instance while a giant kelp located in 10 m of water might have the capacity to sway with a 10 s period to reduce the relative water velocities associated with oceanic swell, due to its great mass and low stiffness it is impossible for such a plant to also oscillate at 1 Hz (or higher frequencies) to ameliorate many of the effects of intertidal flows produced under breaking waves.

A second issue also arises as a consequence of the intertidal-subtidal differences in flow time scales. It is possible that organisms subjected to repeated hydrodynamic forces may become vulnerable to fatigue failure. Sublethal forces can introduce both macroscopic lesions as well as microscopic cracks and stress concentrations within a material (Gordon, 1978). Although many organisms can repair tissues and component structures, damage can also accumulate and propagate through a material with time, particularly if forces are cyclically imposed and removed (Shigley and Mitchell, 1983). Because the time scale of flow variation is 10 times shorter intertidally, this suggests that surf-zone organisms experience an order of magnitude more loading cycles per time than those living subtidally. This effect may act synergistically with the greater magnitude of intertidal flow forces to increase mortality as well as non-lethal tissue loss in surf-zone plants and animals. To date, however, this possibility has received little attention.

5.4.4. Turbulence

Previous studies have shown that energy dissipation rates (an index of turbulence intensity) in the upper layers of the oceans typically vary from 10^{-10} to 10^{-4} W/kg (Baker and Gibson, 1987). These values are miniscule compared to dissipation rates under breaking waves, which have been measured to be as large as 0.05 W/kg on smooth sandy beaches (George et al., 1994) and may reach even larger values on steep rocky shores (Gaylord and Mead, in prep.). Such large dissipation rates can affect organisms directly. For example, Mead and Denny (1995) have shown that the viscous fluid shear associated with turbulent energy dissipation can decrease fertilization efficiency of the purple sea urchin, *Strongylocentrotus purpuratus*, (which engages in external fertilization) by interfering with the interaction of sperm and egg. Although energy dissipation rates in the subtidal benthic boundary layer may also be large, such values are confined to regions within a few centimeters of the bottom rather than extending throughout the water column as in intertidal regions. High turbulence levels can also increase rates of mixing and dispersion (Csanady, 1973), with numerous additional biological implications beyond the scope of this study.

5.4.5. Emersion and wave impact

Due to the rise and fall of the tides, organisms living intertidally may not only experience rapid flows from breaking waves; they may also experience conditions of zero flow. For organisms that depend on water motion for delivery of food or removal of wastes, or are temperature or desiccation sensitive, low tide may therefore represent a period of physiological (as opposed to physical) stress (e.g., Bell, 1993). Perhaps equally importantly, as the tide rises and begins to cover exposed organisms, they may be subjected to severe impact-type forces. An emersed organism hit by the plunging crest of a breaking wave has no surrounding liquid to cushion it, and it appears that such impact-type forces may impose some of the largest loads encountered by many plants and animals (Gaylord, in prep.). In contrast, organisms living subtidally avoid impact loads altogether.

5.5. Caveats and conclusions

Development of the above flow data has relied on several assumptions, the most important of which relate to the extraction of time series of velocity and acceleration from measurements of force. Eqs. 7 and 8 assume that the hydrodynamic forces imposed on a flow probe are composed of the sum of drag and hydrodynamic accelerational forces, with constant coefficients (C_d and C_a) and negligible lift. In flows that rapidly change direction and magnitude or that are highly turbulent (all of which are true in the surf zone), vortex and wake effects can become important, and may therefore complicate relationships between velocity/acceleration and force by altering C_d and C_a. Also, although lift was minimized by using a radially-symmetrical drag element, strongly nonuniform flows can generate lift even on perfect spheres (Miloh, 1994). These effects indicate that the results presented here should be viewed as quantitative estimates, rather than precision recordings, of surf-zone velocities and accelerations.

It should also be noted that these flow data provide information regarding temporal variation of velocity and acceleration at only a single point in space. As such, the recordings do not describe the overall spatial structure of the flow fields produced under breaking waves. In particular, components of acceleration that derive from the temporal variation in velocity become difficult to distinguish from those arising from the advection of spatial gradients in velocity. Such details can be important; a more complete examination of the spatial character of surf-zone accelerations suggests that their length scales are sufficiently small (order 1 cm) that their role in imposing forces on many intertidal organisms may be minimal. Thus, although the data of Figs. 15–17 may be useful in predicting simultaneous relative vectors of velocity and acceleration occurring at a point (rather than a region of space), caution must be employed when attempting to estimate hydrodynamic consequences of these flows for organisms of finite size. Unfortunately, this topic requires more discussion than what is possible here and will therefore be addressed in detail in a separate paper (Gaylord, in prep.).

Despite the presence of these complicating factors, the measurements and relationships presented in this report provide substantially more information than has been available to date concerning the nature of surf-zone flows on rocky shores. In particular, they provide a first detailed exploration of the magnitudes of water velocity and

acceleration as a function of wave height, and provide a first quantitative glimpse of the stochastic variation in maximal flows produced by waves of given size. The present recordings also yield the missing description of how simultaneous magnitudes of velocity and acceleration may be related. As such, the measurements of this study set the stage for a more complete examination of a wide variety of hydrodynamic consequences for the organisms that live in the pounding surf of the wave-swept environment.

Acknowledgements

I thank M.W. Denny for field and lab assistance, valuable discussions, and critical feedback. J. Leichter, G. Villa, L. Roberson, B. Hunt, and L. Hunt assisted with diving. R. Phillips and the Monterey Bay Aquarium kindly lent their subtidal wave height recorder, and J. Watanabe generously shared personal data. S. Thompson provided temporary lab space for use as a monitoring station. I also am grateful to Mimi Koehl and an anonymous reviewer for constructive and helpful comments on the manuscript. This work was supported by NSF grant OCE-9313891 to M.W. Denny.

References

Baker, M.A., Gibson, C.H., 1987. Sampling turbulence in the stratified ocean: statistical consequences of strong intermittency. J. Phys. Oceanogr. 17, 1817–1836.

Batchelor, G.K., 1967. An Introduction to Fluid Dynamics, Cambridge University Press, Cambridge.

Bell, E.C., 1993. Photosynthetic response to temperature and desiccation of the intertidal alga *Mastocarpus papillatus*. Mar. Biol. 117, 337–346.

Bell, E.C., Denny, M.W., 1994. Quantifying ''wave exposure'': a simple device for recording maximum velocity and results of its use at several field sites. J. Exp. Mar. Biol. Ecol. 181, 9–29.

Bendat, J.S., Piersol, A.G., 1986. Random Data: Analysis and Measurement Procedures, 2nd ed, John Wiley & Sons, New York.

Blanchette, C.A., 1997. Size and survival of intertidal plants in response to wave action: a case study with *Fucus gardneri*. Ecology 78, 1563–1578.

Brodersen, K.P., 1995. The effect of wind exposure and filamentous algae on the distribution of surf zone macroinvertebrates in Lake Esrom, Denmark. Hydrobiologia 297, 131–148.

Connell, J.H., 1978. Diversity in tropical rain forests and coral reefs. Science 199, 1302–1310.

Csanady, G.S., 1973. Turbulent Diffusion in the Environment, D. Reidel, Boston.

Dayton, P.K., 1971. Competition, disturbance, and community organization: the provision and subsequent utilization of space in a rocky intertidal community. Ecol. Monogr. 41, 351–389.

Dayton, P.K., 1975. Experimental evaluation of ecological dominance in a rocky intertidal algal community. Ecol. Monogr 45, 137–159.

Denny, M.W., 1985. Wave forces on intertidal organisms: a case study. Limnol. Oceanogr. 30, 1171–1187.

Denny, M.W., 1987. Life in the maelstrom: the biomechanics of wave-swept rocky shores. Trends Ecol. Evol. 2, 61–66.

Denny, M.W., 1988. Biology and the Mechanics of the Wave-swept Environment, Princeton University Press, Princeton.

Denny, M.W., 1995. Predicting physical disturbance: mechanistic approaches to the study of survivorship on wave-swept shores. Ecol. Monogr. 65, 371–418.

Denny, M.W., Daniel, T.L., Koehl, M.A.R., 1985. Mechanical limits to size in wave-swept organisms. Ecol. Monogr. 55, 69–102.

Denny, M.W., Gaylord, B., 1996. Why the urchin lost its spines: hydrodynamic forces and survivorship in three echinoids. J. Exp. Biol. 199, 717–729.

Denny, M.W., Gaylord, B., Cowan, E.A., 1998a. Flow and flexibility II: the roles of size and shape in determining wave forces on the bull kelp, *Nereocystis luetkeana*. J. Exp. Biol. 200, 3165–3183.

Denny, M.W., Gaylord, B., Helmuth, B., Daniel, T.L., 1998b. The menace of momentum: dynamic forces on flexible organisms. Limnol. Oceanogr. 43, 955–968.

Donelan, M.A., Motycka, J., 1978. Miniature drag sphere velocity probe. Rev. Sci. Instrum. 49, 298–304.

Doty, M.S., 1971. Measurement of water movement in reference to benthic algal growth. Bot. Mar. 14, 32–35.

Gaylord, B., Blanchette, C.A., Denny, M.W., 1994. Mechanical consequences of size in wave-swept algae. Ecol. Monogr. 64, 287–313.

Gaylord, B., Denny, M.W., 1998. Flow and flexibility I: effects of size, shape, and stiffness in determining wave forces on the stipitate kelps, *Eisenia arborea* and *Pterygophora californica*. J. Exp. Biol. 200, 3141–3164.

George, R., Flick, R.E., Guza, R.T., 1994. Observations of turbulence in the surf zone. J. Geophys. Res. 99, 801–810.

Gerard, V.A., 1982. In situ water motion and nutrient uptake by the giant kelp *Macrocystis pyrifera*. Mar. Biol. 69, 51–54.

Gordon, J.E., 1978. Structures, Da Capo, New York.

Hedges, T.S., Kirkgoz, M.S., 1981. An experimental study of the transformation zone of plunging breakers. Coastal Eng. 4, 319–333.

Hibberd, S., Peregrine, D.H., 1979. Surf and run-up on a beach: a uniform bore. J. Fluid Mech. 95, 323–345.

Horowitz, P., Hill, W., 1989. The Art of Electronics, 2nd ed, Cambridge University Press, Cambridge.

Hughes, S.A., Borgman, L.E., 1987. Beta–Rayleigh distribution for shallow water wave heights. In: Dalrymple, R.A. (Ed.), Proceedings sponsored by the Waterway, Port, Coastal and Ocean Division of ASCE, Coastal Hydrodynamics, ASCE, New York, pp. 17–31.

Hummon, W.D., 1989. The fetch-energy index: an a prior estimator of coastal exposure, applied to littoral marine Gastrotricha of the British Isles. In: Ryland, J.S., Tyler, P.A. (Eds.), Reproduction, Genetics and Distributions of Marine Organisms. 23rd European Marine Biology Symposium, Olsen and Olsen, Fredensborg, Denmark, pp. 387–393.

Jones, W.E., Demetropoulos, A., 1968. Exposure to wave action: measurements of an important ecological parameter on rocky shores of Anglesey. J. Exp. Mar. Biol. Ecol. 2, 46–63.

Keller, H.B., Levine, D.A., Whitham, G.B., 1960. Motion of a bore over a sloping beach. J. Fluid Mech. 7, 302–316.

Kinsman, B., 1965. Wind Waves, Prentice-Hall, Englewood Cliffs.

Koehl, M.A.R., 1977. Effects of sea anemones on the flow forces they encounter. J. Exp. Biol. 69, 87–105.

Koehl, M.A.R., 1982. The interaction of moving water and sessile organisms. Sci. Amer. 247, 124–134.

Koehl, M.A.R., 1984. How do benthic organisms withstand moving water? Amer. Zool. 24, 57–70.

Koehl, M.A.R., 1986. Seaweeds in moving water: form and mechanical function. In: Givnish, T.J. (Ed.), On the Economy of Plant Form and Function, Cambridge University Press, Cambridge, pp. 603–634.

Koehl, M.A.R., Alberte, R.S., 1988. Flow, flapping, and photosynthesis of *Nereocystis luetkeana*: a functional comparison of undulate and flat blade morphologies. Mar. Biol. 99, 435–444.

Komar, P.D., 1976. Beach Processes and Sedimentation, Prentice-Hall, Englewood Cliffs.

Leigh, E.G., Paine, R.T., Quinn, J.F., Suchanek, T.H., 1987. Wave energy and intertidal productivity. Proc. Nat. Acad. Sci. USA 84, 1314–1318.

LeMehaute, B., Divoky, D., Lin, A., 1968. Shallow water waves: a comparison of theories and experiments. Proc. Coastal Eng. Conf. 11, 86–107.

Levin, S.A., Paine, R.T., 1974. Disturbance, patch formation, and community structure. Proc. Natl. Acad. Sci. USA 71, 2744–2747.

Levin, S.A., Paine, R.T., 1975. The role of disturbance in models of community structure. In: Levin, S.A. (Ed.), Ecosystem Analysis and Prediction, Society for Industrial and Applied Mathematics, Philadelphia, pp. 56–67.

Lewis, J.R., 1964. Ecology of Rocky Shores, English Universities Press, London.

Lewis, J.R., 1968. Water movements and their role in rocky shore ecology. Sarsia 34, 13–36.

Longuet-Higgins, M.S., 1952. On the statistical distribution of the heights of sea waves. J. Mar. Res. 3, 245–266.
Longuet-Higgins, M.S., 1980. On the distribution of the heights of sea waves: some effects of nonlinearity and finite band width. J. Geophys. Res. 85, 1519–1523.
Lubchenco, J., Menge, B.A., 1978. Community development and persistence in a low rocky intertidal zone. Ecol. Monogr. 59, 67–94.
McCowan, J., 1891. On the solitary wave. Phil. Mag. 32, 45–58.
McEachreon, J.C.T., Thomas, M.L.H., 1987. Attachment strength of *Ascophylumnodosum* (L.) LeJolis and exposure to wave action. Bot. Mar. 30, 217–222.
McQuaid, C.D., Branch, G.M., 1985. Trophic structure of rocky intertidal communities: response to wave action and implications for energy flow. Mar. Ecol. Prog. Ser. 22, 153–161.
Mead, K.S., Denny, M.W., 1995. The effects of hydrodynamic shear stress on fertilization and early development of the purple sea urchin *Strongylocentrotus purpuratus*. Biol. Bull. 188, 45–56.
Menge, B.A., 1976. Organization of the New England rocky intertidal community: role of predation, competition, and environmental heterogeneity. Ecol. Monogr. 46, 355–393.
Menge, B.A., 1978. Predation intensity in a rocky intertidal community: relation between predator foraging activity and environmental harshness. Oecologia 34, 1–16.
Menge, B.A., Farrell, T.M., 1989. Community structure and interaction webs in shallow marine hard-bottom communities: tests of an environmental stress model. Adv. Ecol. Res. 19, 189–263.
Milne-Thomson, L.M., 1968. Theoretical Hydrodynamics, 5th ed, Dover, New York.
Miloh, T., 1994. Pressure forces on deformable bodies in non-uniform inviscid flows. Q. J. Mech. Appl. Math. 47, 635–661.
Morison, J.R., O'Brien, M.P., Johnson, J.W., 1950. The forces exerted by surface waves on piles. Petroleum Trans. AIME 189, 149–157.
Munk, W.H., 1949. The solitary wave theory and its application to surf problems. Annals New York Acad. Sci. 51, 376–424.
Muus, B.J., 1968. A field method for measuring ''exposure'' by means of plaster balls. Sarsia 34, 61–68.
Nowell, A.R.M., Jumars, P.A., 1984. Flow environments of aquatic benthos. Ann. Rev. Ecol. Syst. 15, 303–328.
Paine, R.T., 1979. Disaster, catastrophe, and local persistence of the sea palm, *Postelsia palmaeformis*. Science 205, 685–687.
Paine, R.T., Levin, S.A., 1981. Intertidal landscapes: disturbance and the dynamics of pattern. Ecol. Monogr. 51, 145–178.
Pond, S., Pickard, G., 1983. Introductory Dynamical Oceanography, 2nd ed, Pergamon Press, Oxford.
Press, W.H., Teukolsky, S.A., Vetterling, W.T., Flannery, B.P., 1992. Numerical Recipes, Cambridge University Press, Cambridge.
Ricketts, E.F., Calvin, J., Hedgpeth, J.W., Phillips, D.W., 1985. Between Pacific Tides, 5th ed, Stanford University Press, Stanford.
Schlichting, H., 1979. Boundary-layer Theory, McGraw-Hill, New York.
Schmidt, R., Oumeraci, H., Partenscky, H., 1992. Impact loads induced by plunging breakers on vertical structures. Coastal Eng. 15, 1545–1559.
Shen, M.C., Meyer, R.E., 1963. Climb of a bore on a beach. Part 2: Non-uniform beach slope. Part 3: Run-up. J. Fluid Mech. 16, 108–125.
Shigley, J.E., Mitchell, L.D., 1983. Mechanical Engineering Design, McGraw-Hill, New York.
Sousa, W.P., 1984. The role of disturbance in natural communities. Ann. Rev. Ecol. Syst. 15, 353–391.
Sousa, W.P., 1985. Disturbance and patch dynamics on rocky intertidal shores. In: Pickett, S.T.A., White, P.S. (Eds.), The Ecology of Natural Disturbance and Patch Dynamics, Academic Press, Orlando, pp. 101–124.
Thomas, M.L.H., 1986. A physically derived exposure index for marine shorelines. Ophelia 25, 1–13.
Thornton, E.B., Guza, R.T., 1982. Energy saturation and phase speeds measured on a natural beach. J. Geophys. Res. 87, 9499–9508.
Thornton, E.B., Guza, R.T., 1983. Transformation of wave height distribution. J. Geophys. Res. 88, 5925–5938.
Underwood, A.J., Jernakoff, P., 1984. The effects of tidal height, wave-exposure, seasonality and rock-pools on grazing and the distribution of intertidal macroalgae in New South Wales. J. Exp. Mar. Biol. Ecol. 75, 71–96.

U.S. Army Corps of Engineers, 1984. Shore protection manual. Dept. of the Army, U.S. Corps of Engineers, Washington.

Utter, B.D., Denny, M.W., 1996. Wave-induced forces on the giant kelp *Macrocystis pyrifera* (Agardh): field test of computational model. J. Exp. Biol. 199, 2645–2654.

Van Dorn, W.G., 1976. Set-up and run-up in shoaling breakers. Proc. 15th Intl. Coastal Eng. Conf., pp. 738–751.

Van Dorn, W.G., 1978. Breaking invariants in shoaling waves. J. Geophys. Res. 83, 2981–2988.

Vogel, S., 1981. Life in Moving Fluids, Princeton University Press, Princeton.